École polytechnique de Louvain

Modelling a dynamic equivalent of active distribution networks for power system frequency and voltage disturbances

Author: **Bryan Kronz**
Supervisors: **Emmanuel De Jaeger, Cyril Cousein**
Readers: **Emmanuel De Jaeger, Cyril Cousein, Bruno Dehez**
Academic year 2022–2023
Master [120] in Electrical Engineering

Abstract

The complexity of distribution power system models is increasing due to the ever-increasing amount of distributed generators connected by power electronics in the distribution network. This leads to unreasonable simulation time for power system planners and operators. This thesis deals with the derivation of a reduced order dynamic equivalent model of a distribution grid with distributed generation. The equivalent model based on the grey-box modelling approach emulates the original unreduced distribution grid model in terms of active and reactive power flow at the point of interconnection with the medium-voltage grid for frequency and voltage stability studies. The model parameters are identified using the Mean-Variance Mapping Optimization algorithm. Particular attention is given to quantifying the accuracy of the model for all disturbances considered. It has been established that for the considered benchmark network, the equivalent model is able to simulate with reasonable accuracy the active and reactive power at the common coupling point about 78% faster than the detailed model. For larger benchmark networks with more distributed generators, the accuracy is still reasonable, and the simulation time gains are even higher.

Acknowledgements

First of all, I would like to thank Professor Emmanuel De Jaeger who made my interest in electrical power systems grow through his excellent courses. Moreover, I would like to thank Professor Emmanuel De Jaeger and Cyril Cousein for having given me the opportunity to work on this subject and for the helpful advices throughout this master thesis.

A special thanks to Dorian Jouret for the great support he gave me during this master. I would also like to thank Alessandro De Luca for lending me his powerful computer to run some heavy simulations.

Last but not least, I would like to thank my family and friends for their support throughout my university years.

Contents

Chapter 1

Introduction

1.1 Background and motivation

It is no secret that over the past decade, the European Union has made numerous efforts to increase its share of renewable energy production. These efforts have been motivated by the desire to limit climate change and improve air quality. Another aim has been to increase the competitiveness of energy prices and reduce dependence on fossil fuels [1]. As a result of the many incentives provided by the EU, the share of renewables in the total energy production has steadily grown from 22% in 2010 to 38% in 2020 as depicted in Figure 1.1.

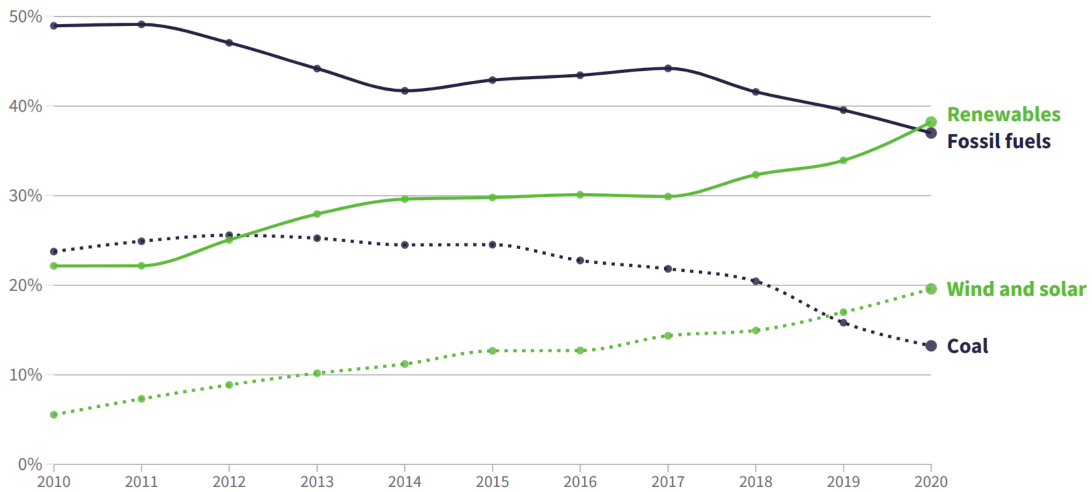

Figure 1.1: Renewables overtake fossil fuels, % share of electricity production in EU-27 (Source: EMBER[2])

This growth is mainly due to the increase in production using solar and wind energy, as it can be seen in Figure 1.2. Among the EU's new incentives to increase the share of renewable energy is a plan to make it mandatory to install solar panels on the roofs of new public and commercial buildings by 2027 and residential buildings by 2029 [3]. In Belgium, rooftop installed solar panels already account for the majority of photovoltaic installations [4]. Therefore, it goes without saying that the number of solar photovoltaic systems connected in the distribution grid will continue to increase.

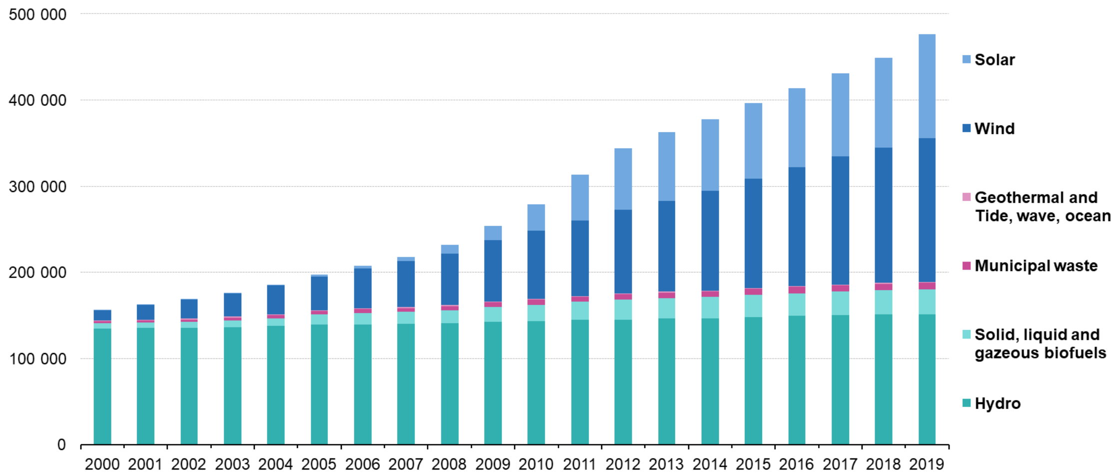

Figure 1.2: Evolution of net maximum electrical capacity for renewables and renewable waste in EU-27 (MW), 2009-2019 (Source: Eurostat[5])

However, the increasing use of renewable energy generators in distribution grids might lead to system stability and security issues. While the grid's dynamics used to be defined by the large synchronous generators at the transmission level, the growing use of inverter-based generators (IBGs) over the last decade makes them now non-negligible from the point of view of system dynamics. In fact, unlike conventional generators, renewables are often interfaced to the grid through power electronic inverters. However, the conventional generators, i.e. synchronous generators, provide some inherent system stabilizing features which IBGs do not. Although IBGs can emulate some of the synchronous generators' features, their behaviour is strongly dependent on how they are controlled. For example, synchronous generators having a rotating mass that provides inertia are naturally able to support the grid in case of frequency perturbations. This is not the case for IBGs. In contrast, the IBG can to some extent emulate this behaviour by changing its active power output as soon as the disturbance is detected. Note however, that the IGBs can easily decrease the power output, but increasing it is often not possible, because of on one hand, the inverter's current capacity limitation and on the other hand, the stochastic nature of the energy source.

In the past, distributed generators were modelled as negative loads. However, given them being more and more present in the grid and their control specific dynamic behaviour, the IGBs must now be modelled properly for accurate results in grid simulations [6]. Unfortunately, this comes at the cost of an increased model complexity that leads to an extended computational time for dynamic simulations. This is specially problematic when simulating large parts of the grid containing a lot of IGBs. A solution to reduce the model complexity and thus the computational time of the simulation is to use a reduced-order equivalent model of the network under study.

1.2 Literature review

Dynamic simulations have for many years been an essential tool for assessing the stability and security of power systems. These simulations are generally performed by power system planners and operators using mathematical models with software products such as MATLAB Simulink®. With the generalized use of distributed generators (DGs) in the grid, there is a shift from the vertically operated power system to a horizontally operated power system. In the vertical system, the electrical system is governed by large centralized generators, while in the horizontal system, the many small and medium-sized generators are distributed over several levels [7] as depicted in Figure 1.3.

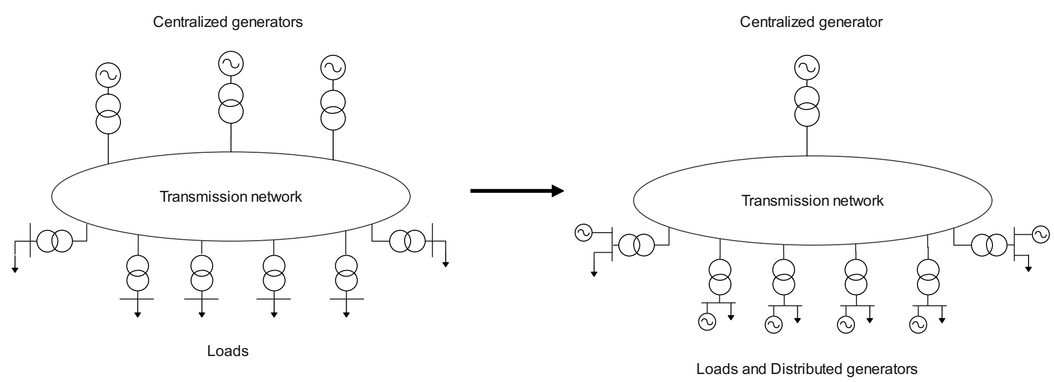

Figure 1.3: Vertical operated power systems (left) and horizontal operated power systems (right)

As already introduced in the last subsection, the control-specific and stochastic behaviour of these, often renewable, distributed generators may affect the overall power system dynamic behaviour. Many efforts have been made in research to overcome the model complexity of the active distribution networks by creating simplified models while trying to maintain accuracy. This literature review mainly relies on (but is not limited to) the ones carried out by [8], [9] and [10].

The main simplification approaches present in the literature are system reduction and measurement based approaches.

System reduction based approaches

System reduction approaches rely on the grouping and removing of parts of the original full model. The two most popular reduction approaches are:

- Modal Analysis

Modal analysis aims at linearizing the system around a steady state point and disregards the modes having less influence. The preserved modes depend on the phenomena to be studied. Different techniques are used depending on the modes to preserve. The main drawback of these techniques is that creating equivalent linear models, they are not able to imitate the detailed model for large perturbations.

- Coherency based methods

Coherency based methods identify coherent features that exist among generators and group them together into an equivalent generator. Coherence between generators depends on their rotor angle oscillations. Then, loads are aggregated in such a way that the original steady state power flow is maintained. The main drawback of these methods relies on the fact that they are based on conventional power systems with few synchronous generators.

Measurement based approaches

As the name suggests, these approaches use measurements from either simulations or measurements on the actual system. The measurements must come from the interconnection between the part of the system that is to simplify and the rest of the system. The advantage of those approaches is that one doesn't need to have a detailed knowledge of the system to be reduced. Based on the available physical knowledge about the model, measurement based approaches can be divided into black box and grey box modelling approaches.

- Black box modelling approach

The black box approach is used when no knowledge about the structure of the model is known a priori. For this approach, algorithms such as Artificial Neural

Network are used to make the model output the correct signals according to the inputs [11]. The disadvantage of this approach is that it is relatively time-consuming and the validity of the model is limited to the system for which it has been tested.

- Grey box modelling approach

The grey box modelling approach uses some physical aspects of the structure of the model without providing a complete description. The main advantage with respect to the black box model is that one can have a better insight and understanding of the model behaviour. This is of special interest for engineers using those models. On the other hand, a model including the complete description of the physical structure, namely a white box model, is not of interest. In fact, it remains an unreduced model. Besides the important computational complexity of an unreduced model, there is also the possibility of confidentiality issues. It may be that the distribution system operator does not want to share detailed information about distribution networks to the transmission system operators. Grey box models also tackle this issue [12]. It should be mentioned that appropriate model parameterization is essential to achieve accuracy.

Conclusion

Although a significant amount of research work has been done around the topic of dynamic equivalencing for active distribution networks, there are still a number of shortcomings. There is limited access to well approved detailed models of distributed generators connected through power electronics. There is also a lack of widely accepted generic models, including the parameters for those generators. Lastly, despite the fact that there have been several attempts to aggregate distributed generators, there is no commonly accepted methodology [6].

1.3 Problem definition and objective

This thesis is focused on assessing the accuracy of a reduced-order dynamic equivalent model of a power distribution grid containing distributed generators, more specifically, residential solar photovoltaic systems. In particular, the power system is studied in case of frequency and voltage fault events. The use of a reduced-order model aims at reducing the computational complexity and thus the simulation time. The main contribution of this work is to quantify the accuracy over a wide range of disturbances and identify the loopholes and their cause, as well as the simulation time savings that the model reduction has brought. The next chapter will describe in detail the distribution benchmark network which will be used for the assessment of the equivalent model, including the used distributed generation model. To account for the frequent lack of detailed knowledge of the complex distribution network, some parameters such as loads and distributed generator parameters are randomized. Afterwards, Chapter 3 explains the methodology used for the creation of the reduced-order model. Then, in Chapter 4, the algorithm to identify the equivalent model's parameters is described. Finally, Chapter 5 compares the original model with the simplified model's results and analyses the accuracy.

Chapter 2

System description

2.1 Benchmark network

2.1.1 Overview

The benchmark network that has been chosen for the study of distribution grid aggregation is a modified version of the CIGRE residential LV network of the European Benchmark [13] as depicted in Figure 2.1. The MV grid is represented by a 20kV bus using a three-phase voltage source. The voltage source is ideally controllable and balanced. The residential distribution grid is connected to the MV grid through a 20kV/400V Δ-Y transformer rated at 200kVA. The distribution feeder supplies five different residential loads. On each of the nodes containing a load, there is also a photovoltaic generator.

2.1.2 Load and line impedance model

Both the load and line impedance models come from the MATLAB Simulink® Simscape library. The load acts as a constant impedance at nominal frequency. Furthermore, the active and reactive power consumed by the load is proportional to the square of the applied voltage [14]. The line impedance is modelled through the *Three-Phase Series RLC Branch* model [15].

$$
\begin{aligned}
P(V) &= P_0(\frac{V}{V_0})^2 \\
Q(V) &= Q_0(\frac{V}{V_0})^2
\end{aligned}
\tag{2.1}
$$

With P_0 and Q_0 the initial active and reactive power. V_0 and V are the initial and measured terminal voltages.

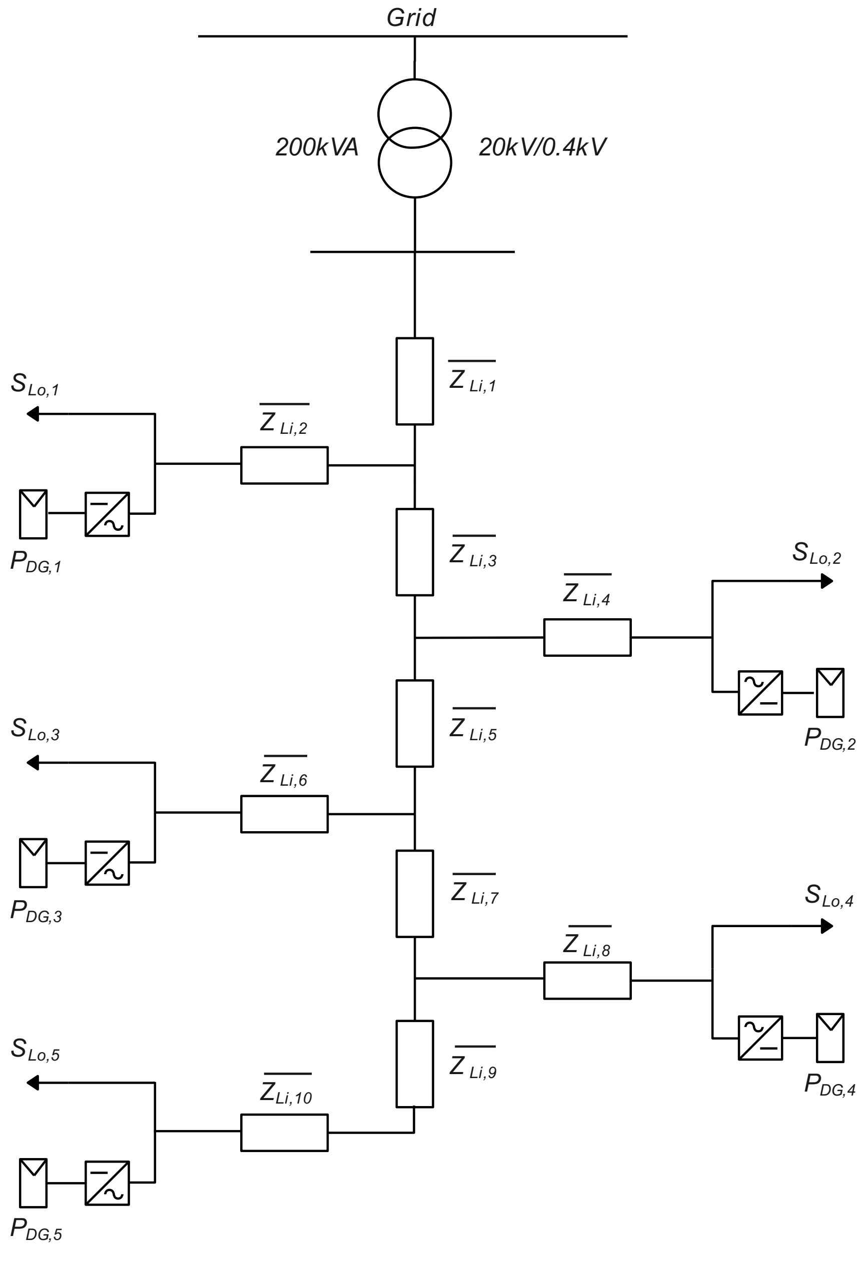

Figure 2.1: Benchmark network

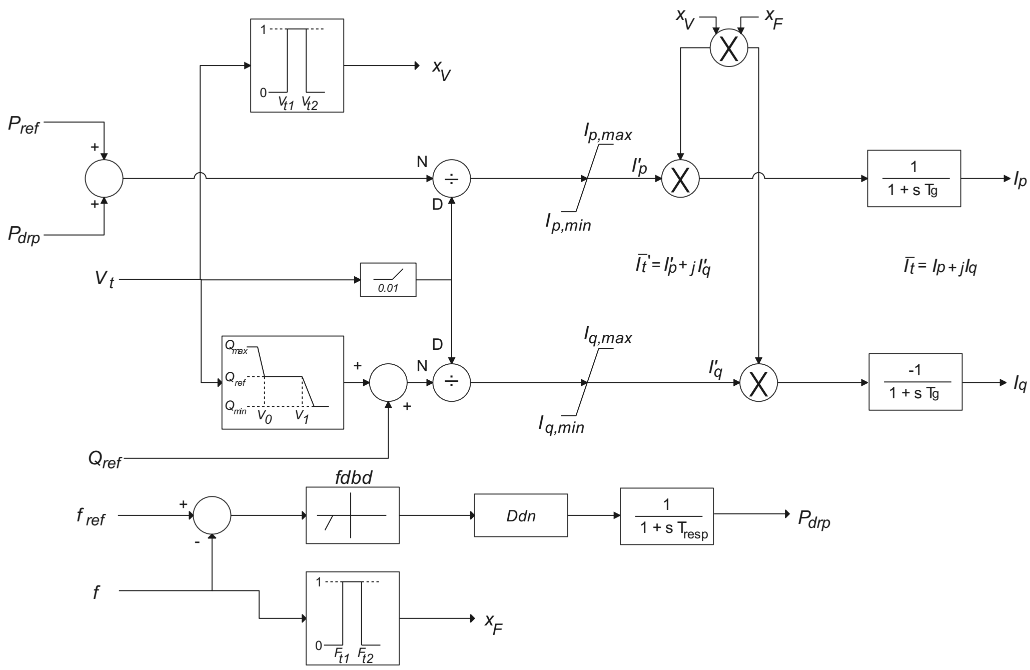

Figure 2.2: Distributed generator model

2.2 Distributed generation model

2.2.1 Model description

The model for the distributed solar power generator is inspired by the model suggested by the Western Electrical Coordinating Council (WECC) that is called *PVD1* [6]. Figure 2.2 depicts the model diagram. The model behaves as a current injector with the ability for active power control, reactive power control and protection. The way that it is has been implemented in this project's Simulink model is the following. The *PVD1* output signals I_p and I_q which account for the active and reactive power to be injected into the grid are converted into an active and reactive power quantity. These quantities are given as inputs to MATLAB Simulink®'s *Three-Phase Dynamic Load* model. Note that some of the model parameters are expressed in per unit on the generator's MVA base. The rest of this subsection explains the different components of the model and its functionalities in detail.

Tripping of the generation based on abnormal frequency or terminal voltage

The system frequency f is measured by the PLL. In case of an under or over-frequency disturbance, the distributed generator (DG) may disconnect for protection purposes. This occurs either if the measured frequency f is below the under-frequency tripping threshold F_{t1} or above the over-frequency tripping threshold F_{t2}. Similarly, if the measured terminal voltage V_t is either below the under-voltage tripping threshold V_{t1} or above the over-voltage tripping threshold V_{t2}, the DG disconnects.

This effect is described by Equation 2.2.

$$\overline{I_t} = \begin{cases} \overline{I_t}' & \text{if } (F_{t1} \leq f \leq F_{t2}) \ \& \ (V_{t1} \leq V_t \leq V_{t2}) \\ 0 & \text{otherwise} \end{cases} \tag{2.2}$$

With $\overline{I_t} = I_p + jI_q$ and $\overline{I_t}'$ the current to be injected before evaluating the tripping logic.

Limited frequency sensitive mode - over frequency (LFSM-O)

The model is able to operate in the limited frequency sensitive mode during over frequency events. In fact, as represented in Equation 2.3, if the difference between the measured frequency f and reference frequency f_{ref} (50 Hz) is above the deadband frequency f_{dbd}, then the active power output of the system is decreased by an amount P_{drp} determined by the over-frequency, the down regulation droop gain Ddn and the response time T_{resp}.

$$P_{drp} = P_{ref}(|f_{ref} - f| - |f_{ref} - f_{dbd}|)Ddn \tag{2.3}$$

With P_{ref} the active power provided by the generator under normal conditions. The response time is modelled by the first order transfer function $\frac{1}{1+sT_{resp}}$.

Reactive power support

The model allows injecting reactive power during steady state (V-Q control), thus operating at non unity power factor, by setting the reference reactive power parameter Q_{ref}.

Moreover, the model also supports reactive current injection during network disturbances. This functionality can be set by the user with help of the following parameters. The lower and upper limit of deadband for the voltage droop response V_0 and V_1, the minimum and maximum reactive power command Q_{mn} and Q_{mx} and the voltage droop response characteristic $Dqdv$. However, to inject reactive current, the active power output has to be lowered not to exceed the inverter current capacity. The active power reduction is done according to the following equation.

$$I_{p,max} = \sqrt{I_{max}^2 - I_q^2} \tag{2.4}$$

With $I_{p,max}$ the active current limit, I_q the reactive current and I_{max} the apparent maximum current. In practice, I_{max} is a limitation related to the inverter current capacity.

Although reactive power support for PV generators has already been extensively investigated [16], the recent Belgian grid code does not require it for small generators (<1MW) [17]. Also, PV systems connected in the distributed grid usually operate at unity power factor [6]. Therefore, in the framework of this project, Q_{ref}, Q_{mn} and Q_{mx} are fixed to 0.

Phase-locked loop (PLL)

The phase-locked loop (PLL) measures the grid phase angle and frequency. In the case of inverter-based generators, the correct grid phase angle and frequency estimation is necessary to inject power with the desired power factor. Furthermore, in case of large frequency deviations, the frequency measurements are important for the activation of the limited frequency sensitive mode or for the tripping of the generator for protection. The following model depicted in Figure 2.3 from [18] has been implemented in this work. $k_{p,PLL}$ and $k_{i,PLL}$ are PI controller constants and w_c the cut-off frequency of the low-pass filter.

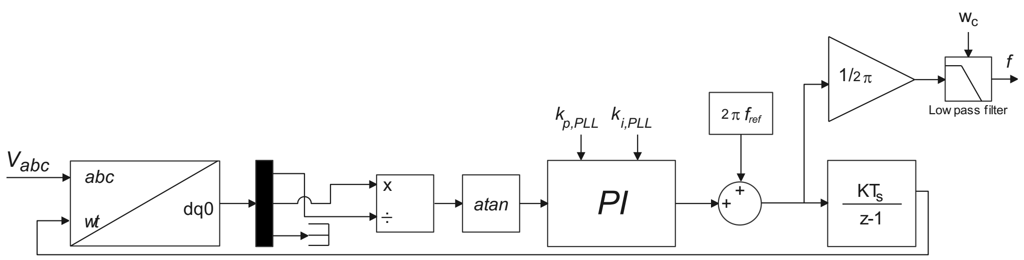

Figure 2.3: Phase-locked loop model

Inverter current lag

The inverter current lag is modelled by the transfer function $\frac{1}{1+sT_g}$ with T_g the inverter current lag time constant (0.02 s).

2.2.2 Parameter values

Line impedance

The line parameters are given in Table 2.1 according to [13]. Their impedance is computed as follows.

$$\overline{Z_{Li,i}} = l_{Li,i}(R'_{Li,i} + j2\pi f L'_{Li,i}) \tag{2.5}$$

Table 2.1: Line parameters

Line number i	$R'(\Omega/\text{km})$	$L'(\text{H/km})$	$l(\text{m})$
1	0.162	0.223	35
2	1.539	0.242	30
3	0.162	0.223	35
4	0.265	0.225	135
5	0.162	0.223	70
6	0.229	0.229	30
7	0.162	0.223	105
8	1.539	0.242	30
9	0.162	0.223	35
10	1.113	0.234	30

Load impedance

The loads' apparent power $|S_{Lo,i}|$ is initialized by randomly generating for each load $i \in \{1, 2, 3, 4, 5\}$ a value in [10kVA; 60kVA] with a power factor $cos(\phi)$ of 0.95. The load's impedances are computed in the following manner.

$$\overline{Z_{Lo,i}} = \frac{V_{LV}^2}{(P_{Lo,i} + jQ_{Lo,i})^*} \tag{2.6}$$

With $V_{LV} = 400V$, $P_{Lo,i} = |S_{Lo,i}|cos\phi$ and $Q_{Lo,i} = |S_{Lo,i}|sin\phi$.

Distributed generators parameters

The amount of active power supplied by each distributed generator $P_{DG,i}$ is initialized by randomly generating a value as being between 10% and 50% of the active power consumed by the load at that same node, as indicated in Equation 2.7. The PV generators operate at a power factor of 1, so the reactive power generation is zero. In addition, the simulation time of the model is assumed to be short enough for the load and power generation reference to remain constant during it.

$$\begin{cases} P_{DG,i} = \texttt{rand}(0.1; 0.5) P_{Lo,i} \\ Q_{DG,i} = 0 \end{cases} \quad \text{for } i \in \{1,2,3,4,5\} \tag{2.7}$$

With rand(x,y) a function that generates a random number between x and y.

The model is set to comply with the recent Belgian grid code requirements for Type A generators [17]. Type A generators are defined to have a maximum capacity between 0.8kW and 1MW. According to the recent grid code, the generator should stay connected inside the range of frequencies [47.5Hz;51.5Hz]. Moreover, the LFSM-O should be activated at the threshold value of 50.2Hz. While in this mode, the active power output is reduced according to a down regulation droop s_{LFSM} value between 2% and 12%. The active power reduction response time should occur as fast as possible. To account for different response capabilities due to technology differences, the response time T_{resp} for each generator is set between 0.00s and 0.06s. Note that the down regulation droop Ddn defined in Equation 2.3 is slightly different from the one commonly defined in grid codes. Indeed, the conventional down regulation droop s_{LFSM} is defined as follows [19].

$$s_{LFSM} = \frac{|f_{ref} - f| - |f_{ref} - f_{dbd}|}{f_{ref}} \frac{P_{ref}}{P_{drp}} \tag{2.8}$$

Equation 2.3 and 2.8 give the relationship between the two quantities.

$$Ddn = \frac{1}{s_{LFSM} f_{ref}} \tag{2.9}$$

Therefore, to have s_{LFSM} in the range $[0.02; 0.12]$, Ddn must be in the range $[0.167; 1]$

Table 2.2 gives the DG's parameter ranges. Those parameters are randomly generated inside their respective range. Note that "p.u. on mbase" means per unit on the generator apparent power.

Table 2.2: Distributed generator parameter ranges

Parameter	Range	Unit
F_{t1}	[46.5;47.5]	Hz
F_{t2}	[51.5;52.5]	Hz
V_{t1}	[0.88;0.90]	p.u.
V_{t2}	[1.10;1.20]	p.u.
V_0	-	p.u.
V_1	-	p.u.
Q_{mn}	[0;0]	p.u. on mbase
Q_{mx}	[0;0]	p.u. on mbase
Ddn	[0.167;1.00]	$\frac{1}{Hz}\cdot$ p.u. on mbase
T_{resp}	[0.00;0.06]	s
f_{dbd}	[0.2;0.2]	Hz

Phase-locked loop

Each of the distributed generators PLL has their parameters randomly generated inside their respective range as depicted in Table 2.3 [18].

Table 2.3: PLL parameter ranges

Parameter	Range	Unit
$k_{p,PLL}$	[60;120]	Hz
$k_{i,PLL}$	[600;1200]	Hz
w_c	[10π;20π]	rad/s

Chapter 3

Reduced-order system description

The ideal way to accurately represent the dynamic behaviour of a network containing multiple DGs is to model each DG individually. However, as the amount of DGs in a system grows, the computational load dramatically increases. Aggregating together individual DGs into an equivalent distributed generator is a solution to achieve a balance between accuracy and computational complexity [6]. To do so, the load and line impedance also need to be aggregated. Figure 3.1 depicts the aggregation of the detailed model into the reduced-order model. This chapter describes the methodology used to obtain the equivalent load, line impedance and aggregated DG. In particular, the equivalent or aggregated model is designed to behave like the original detailed model in terms of active and reactive power flow at the point of common coupling (PCC).

3.1 Equivalent load and line impedance

The total equivalent system impedance is obtained as follows [18].

$$\begin{aligned}
\overline{Z_{equ,1}} &= (\overline{Z_{Lo,5}} + \overline{Z_{Li,10}} + \overline{Z_{Li,9}})//(\overline{Z_{Li,8}} + \overline{Z_{Lo,4}}) \\
\overline{Z_{equ,2}} &= (\overline{Z_{equ,1}} + \overline{Z_{Li,7}})//(\overline{Z_{Lo,3}} + \overline{Z_{LI,6}}) \\
\overline{Z_{equ,3}} &= (\overline{Z_{equ,2}} + \overline{Z_{Li,5}})//(\overline{Z_{Li,4}} + \overline{Z_{Lo,2}}) \\
\overline{Z_{equ,tot}} &= [(\overline{Z_{equ,3}} + \overline{Z_{Li,3}})//(\overline{Z_{Lo,1}} + \overline{Z_{Li,2}})] + \overline{Z_{Li,1}}
\end{aligned} \tag{3.1}$$

The equivalent load impedance is obtained as the following.

$$\overline{Z_{equ,load}} = \left[\sum_{i=1}^{5} \frac{1}{\overline{\overline{Z_{Lo,i}}}}\right]^{-1} \tag{3.2}$$

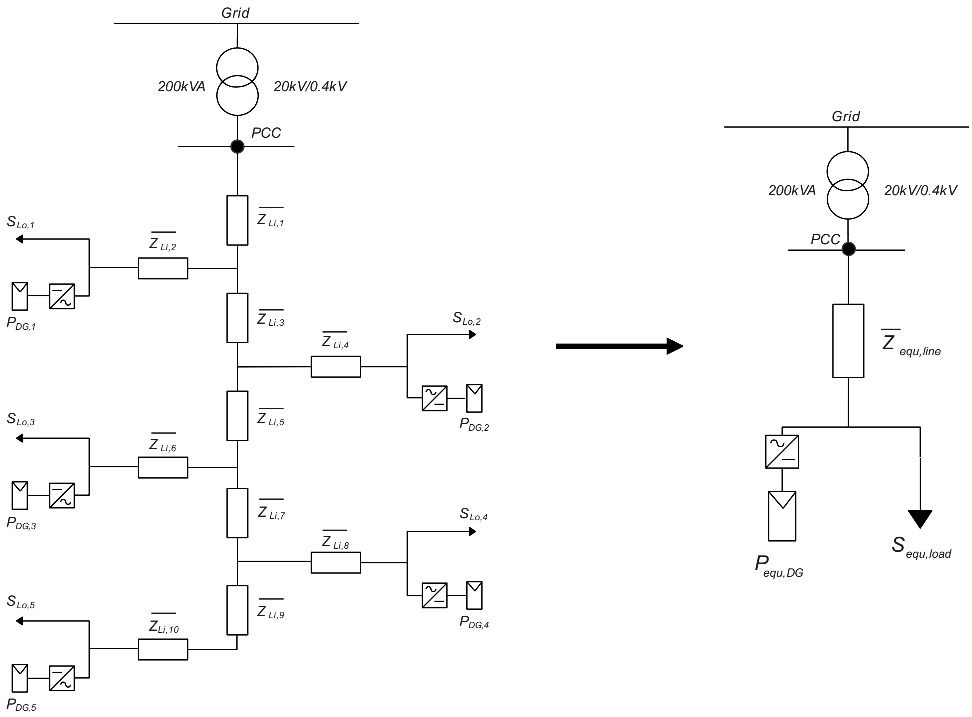

Figure 3.1: Detailed system model to reduced-order model

The equivalent load apparent power is given as follows.

$$S_{equ,load} = \frac{V_{LV}^2}{\overline{Z_{equ,load}}^*} \tag{3.3}$$

Finally, with Equation 3.1 and 3.2 the equivalent line impedance is computed.

$$\overline{Z_{equ,line}} = \overline{Z_{equ,tot}} - \overline{Z_{equ,load}} \tag{3.4}$$

3.2 Aggregated distributed generation

The aggregated model should be able to emulate the influence of all the individual distributed generators. In particular, the tripping of the generation and the over-frequency response ancillary service.

The aggregated power generation is computed as follows.

$$P_{equ,DG} = \sum_{i=1}^{5} P_{DG,i} \tag{3.5}$$

The partial tripping logic allows taking into account the tripping of individual DGs into a single DG [6]. For example, in the case of a severe under-frequency event, the power output is diminished by a certain amount to emulate the tripping of some but not all the generators. The decrease in generation of the aggregated DG is linear. The complete partial tripping logic is described by Equation 3.6, 3.7, 3.8 and illustrated by the blue blocks in the aggregated distributed generator model in Figure 3.2.

$$\overline{I_t} = \overline{I_t}' x_F x_V \tag{3.6}$$

With

$$x_F = \begin{cases} 1 & \text{if } F_{pt1} \leq f \leq F_{pt2} \\ \frac{f - F_{pt0}}{F_{pt1} - F_{pt0}} & \text{if } F_{pt0} < f < F_{pt1} \\ \frac{-(f - F_{pt3})}{F_{pt3} - F_{pt2}} & \text{if } F_{pt2} < f < F_{pt3} \\ 0 & \text{otherwise} \end{cases} \tag{3.7}$$

And

$$x_V = \begin{cases} 1 & \text{if } V_{pt1} \leq V_t \leq V_{pt2} \\ \frac{V_t - V_{pt0}}{V_{pt1} - V_{pt0}} & \text{if } V_{pt0} < V_t < V_{pt1} \\ \frac{-(V_t - V_{pt3})}{V_{pt3} - V_{pt2}} & \text{if } V_{pt2} < V_t < V_{pt3} \\ 0 & \text{otherwise} \end{cases} \tag{3.8}$$

With F_{pt0}, F_{pt1}, F_{pt2}, F_{pt3} partial tripping thresholds due to over/under-frequency and V_{pt0}, V_{pt1}, V_{pt2}, V_{pt3} partial tripping thresholds due to over/under terminal voltage.

The above parameters, related to the partial tripping and the remaining DG parameters (including PLL), need to be adequately identified. The parameter identification methodology is explained in the next chapter.

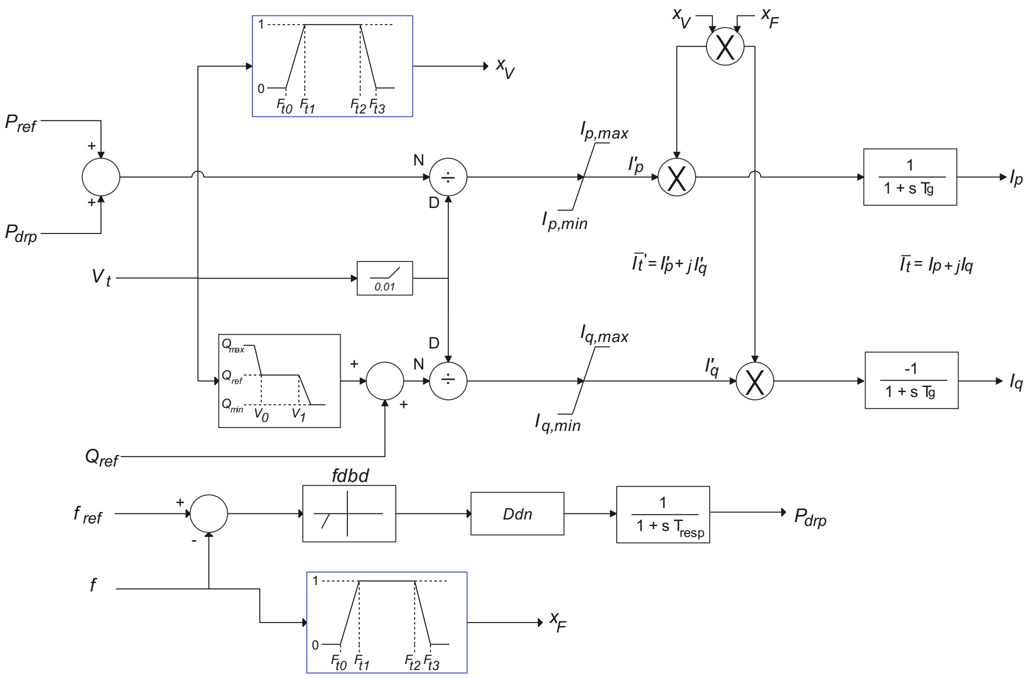

Figure 3.2: Aggregated distributed generator model

Chapter 4

Reduced-order model parameter identification

The right parameters are needed to be given to the equivalent model for it to correctly mimic the detailed model's behaviour. The detailed model has several distributed generators (DGs), with each of them having different parameters strongly influencing the dynamic behaviour. The equivalent model has only one DG, which aggregates all the DGs from the detailed model. Therefore, this is not a trivial task.

The most widespread parameter identification techniques are based on the well-known Monte Carlo simulations [20]. Some other parameter identification techniques that have been used within the power systems' context are:

- The Extended Two Particle Swarm Optimization [21](2007)
- Differential Evolutionary Particle Swarm Optimization [22](2013)
- Mean-variance mapping optimization algorithm [23](2017)
- Evolutionary Deep Reinforcement Learning [24](2020)

The Mean-variance mapping optimization (MVMO) has been chosen to be implemented in this work.

4.1 Mean-variance mapping optimization algorithm

The MVMO algorithm is used here in the framework of identifying parameters of a dynamic equivalent of an active distribution network. The flowchart in Figure 4.1 illustrates the algorithm's operation.

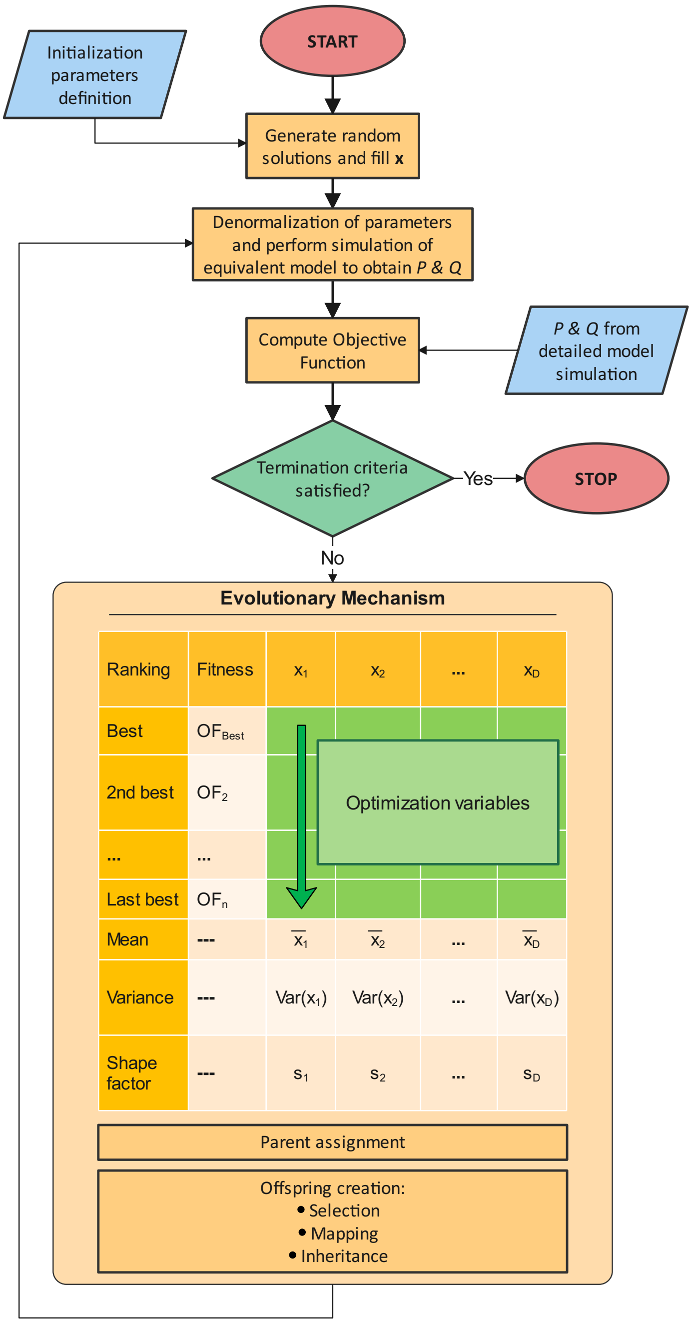

Figure 4.1: Mean-variance mapping optimization algorithm flowchart

First, a set of algorithm initialization parameters are defined. The archive size n, the maximum number of function evaluations $MaxEval$, the number of randomly varied variables m and the parameter's range $[min_j, max_j]$ for each of the estimated parameters $\{x_j,\ j \in \{1, ..., D\}\}$. Then, the equivalent model's parameters to be determined are randomized in the interval $[0; 1]$ and the solution vector $\mathbf{x}$ is filled with them. Afterwards, the estimated parameters are denormalized as follows.

$$\tilde{x_j} = x_j(max_j - min_j) + min_j \tag{4.1}$$

With x_j the j^{th} parameter normalized and $\tilde{x_j}$ denormalized.

Then, the aggregated model simulation is run and the measurements at the point of common coupling (PCC) of the active power P_{agg} and reactive power Q_{agg} are stored. The active power P_{det} and reactive power Q_{det} at the PCC of the detailed model have been stored beforehand. The objective function OF is then computed as in Equation 4.2. Note that the active and reactive power are evaluated in the dynamic range.

$$OF = \alpha_k \sum_{k=1}^{K} \left\{ \frac{1}{N} \sum_{i=1}^{N} \left[(P_{agg,k,i} - P_{det,k,i})^2 + (Q_{agg,k,i} - Q_{det,k,i})^2 \right] \right\} \tag{4.2}$$

With:

- K the number of disturbances evaluated
- α_k the probability of the k^{th} disturbance
- $N = t_{eval}/T_s$ with t_{eval} the evaluated time interval and T_s the simulation step size

The solution vector $\mathbf{x}$ with the lowest associated OF, i.e. the set of estimated parameters having the best fitness, are stored in an archive of size n. This keeps track of the best n solution vectors $\mathbf{x}$ so far. In this archive, the mean $\overline{x_j}$, variance $Var(x_j)$ and shape factor s_j of each parameter x_j among the n best solution vectors $\mathbf{x}$ are computed. These quantities are used in the Evolutionary Mechanism. The shape factor is computed as follows.

$$s_j = -\ln(Var(x_j)) \tag{4.3}$$

During the Evolutionary Mechanism, the solution vector with the best OF $\mathbf{x}_{Best}$ is assigned as the parent. Then, the offspring creation takes place in three steps: the selection, the mapping and the inheritance. The selection is a procedure that randomly chooses a number m of parameters to be changed. Next, the selected parameters values are mapped according to the h-function variables, as the following system of equations shows.

$$\begin{cases} h(\bar{x_j}, s_j, u_j) = \bar{x_j}(1 - e^{-u_j s_j}) + (1 - \bar{x_j})e^{-(1-u_j)s_j} \\ x_j = h_x + (1 - h_1 + h_0)x'_j - h_0 \end{cases} \tag{4.4}$$

With $h_x = h(u_j = x'_j)$, $h_0 = h(u_j = 0)$, $h_1 = h(u_j = 1)$ and $x'_j \in [0, 1]$ a random number

Equation 4.4 output x_j is in $[0; 1]$, thus the created offspring will not be outside its fixed range.

The remaining parameters $D - m$, which were not changed during the offspring creation, get their respective value from $\mathbf{x}_{Best}$. Next, the algorithm starts over. Finally, the algorithm stops when the end criterium is reached.

4.2 Estimated parameters

The reduced-order model's parameters to be estimated, and their ranges, are given in Table 4.1.

Table 4.1: Estimated parameters

Parameter number j	**parameter** x_j	**range** $[max_j;min_j]$	Unit
1	F_{pt0}	[46.5;47.5]	Hz
2	F_{pt1}	[46.5;47.5]	Hz
3	F_{pt2}	[51.5;52.5]	Hz
4	F_{pt3}	[51.5;52.5]	Hz
5	V_{pt0}	[0.70;1.00][1]	p.u.
6	V_{pt1}	[0.70;1.00][1]	p.u.
7	V_{pt2}	[1.00;1.30][1]	p.u.
8	V_{pt3}	[1.00;1.30][1]	p.u.
9	Ddn	[0.167;1.00]	$\frac{1}{Hz}\cdot$ p.u. on mbase
10	T_{resp}	[0.00;0.06]	s
11	$k_{p,PLL}$	[60;120]	Hz
12	$k_{i,PLL}$	[600;1200]	Hz
13	w_c	$[10\pi;20\pi]$	rad/s

4.3 Further discussion

4.3.1 Note on the Evolutionary Mechanism

The particularity of this algorithm is that thanks to the Evolutionary Mechanism, it makes "smart guesses" instead of totally random attempts in order to find parameter values minimizing the error between the simplified and detailed model. The guesses are qualified as smart, because although randomness is involved, they are based on statistical quantities of previous trials.

For the sake of simplicity, let's take a situation in which the mean $\bar{x}$ of the stored n values of a parameter is equal to 0.5 and assume that this parameter has been selected to be mapped according to the h-function. Depending on the on variance the of the stored values of this parameter, the possible mapping outcomes

[1] The identified parameter range is the same as the range in which the detailed model parameters were generated, expect for $Vpt0$, $Vpt1$, $Vpt2$ and $Vpt3$. For those parameters, a broader range is chosen, because depending on the network architecture, the terminal voltage can vary from one DG to another for a given bus voltage.

can vary significantly. Figure 4.2 illustrates the h-function for different shape factor values. The shape factor value as a function of the variance can be seen in Figure 4.3

One can observe that for a smaller variance, i.e. a greater shape factor, the parameter value will be most probably mapped near around the mean $\bar{x} = 0.5$. On the other hand, if the variance is greater, meaning that the stored values are distanced, the new parameter can be mapped over a larger range. This is because, since the stored values are distanced from each other, it is not obvious which parameter value is the best and more values need to be explored.

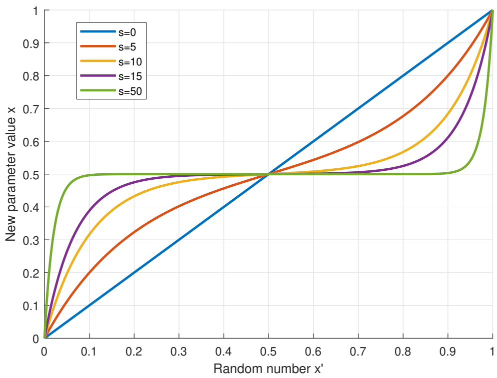

Figure 4.2: h-function for different shape factors

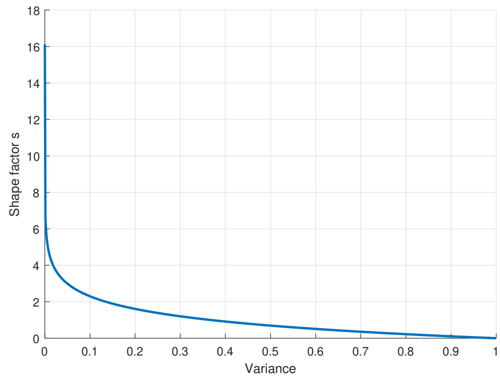

Figure 4.3: Shape factor as a function of the variance

4.3.2 Initialization parameters

- The archive size n needs to be at least of size 2 so that the algorithm works properly [25]. Concerning the upper bound, there is no strict rule, as it won't directly affect the end results. [23], [25], [26], [27] and [28] choose n between 2 and 5. In this work, n has been set to 4.

- The maximum number of function evaluations $MaxEval$ is difficult to set without prior knowledge. As a rule of thumb, [28] chose $MaxEval$ as $50D$, with D the number of parameters to identify. Therefore, in this case, it would be 650. To be on the safe side, the amount of needed evaluations is overestimated and fixed to 1000.

- The number of randomly varied variables m has obviously to be smaller or equal to the total number of parameters D. A smaller m is useful during the first iterations as it can evaluate the parameters in a more isolated way as less of them change from one iteration to another. A bigger m is useful when the algorithm has already made a good amount of evaluations, as it will explore more alternative parameter values at the same time. In this work, m has been fixed to 6.

- The probability of the k^{th} disturbance α_k gives the user the ability to give a higher or lower weight to a disturbance in the objective function. This enables the possibility to make the simplified model fit in priority to some specific disturbances. The goal in this thesis to have an accurate model for any disturbance. Therefore, the weight of any disturbance should be equal. α_k is set to 1/K.

4.3.3 Termination criteria

The termination criteria can be set in three different manners [23]:

- The maximum number of function evaluations $MaxEval$ is reached.
- The objective function OF has not been reduced over a chosen number of evaluations.
- A desired fitness level is reached.

The last option can be translated into the following:

$$OF \leq OF_{termination} \tag{4.5}$$

So that the user can have an idea of the value of $OF_{termination}$ to set, one can attempt to develop Equation 4.5.

$$\begin{aligned} OF_{termination} &= \alpha_k \sum_{k=1}^{K} \left\{ \frac{1}{N} \sum_{i=1}^{N} \left[(P_{agg,k,i} - P_{det,k,i})^2 + (Q_{agg,k,i} - Q_{det,k,i})^2 \right] \right\} \\ &= \alpha_k \sum_{k=1}^{K} \left\{ \frac{1}{N} \sum_{i=1}^{N} (P_{agg,k,i} - P_{det,k,i})^2 + \frac{1}{N} \sum_{i=1}^{N} (Q_{agg,k,i} - Q_{det,k,i})^2 \right\} \end{aligned}$$

With $\alpha_k = \frac{1}{K}$ and the introduction of the mean squared error MSE:

$$OF_{termination} = \frac{1}{K} \sum_{k=1}^{K} \left\{ \mathrm{MSE}_{P,k} + \mathrm{MSE}_{Q,k} \right\}$$

If one fixes the MSE to be constant over any disturbance k:

$$\begin{aligned} OF_{termination} &= \frac{1}{K} K \left\{ \mathrm{MSE}_P + \mathrm{MSE}_Q \right\} \\ &= \mathrm{MSE}_P + \mathrm{MSE}_Q \end{aligned}$$

Lastly, if the same MSE is expected for the active and reactive power:

$$OF_{termination} = 2\text{MSE} \tag{4.6}$$

The problem is that this expression falsely gives the impression that a certain MSE can be expected for active and the reactive power. However, in a reality, it is possible that the $OF_{termination}$ is achieved by having a very low MSE for the reactive power and a higher one for the active power or vice versa. It is not possible to separately set and get an MSE for one or the other.

Finally, the first option has been chosen for this work, i.e. the termination criteria according to $MaxEval$, as it is the safest one according to [23].

Chapter 5

Equivalent model validation and analysis of the results

In this chapter, the results from the simplified model and the detailed model are compared. The comparison is done with respect to the active and reactive power flow at the point of common coupling (PCC) in the case of grid disturbances. The grid disturbances include frequency and voltage deviations.

For this purpose, the detailed model parameters are generated as indicated in Chapter 2 and are given in Appendix A.1. The simplified model equivalent load and line impedance are computed as explained in section 3.1. The aggregated distributed generator parameters are estimated according to the MVMO algorithm described in Chapter 4.

5.1 Error metric

An adequate error metric has to be defined to properly evaluate the accuracy of the reduced-order model. The used parameter estimation algorithm is part of evolutionary algorithms, which are part of heuristic algorithms [29]. This class of algorithms is used both in machine learning and artificial intelligence [30]. In machine learning, the error metrics that are most commonly used for assessing accuracy (for prediction, not classification) are the root mean squared error (RSME) and the mean absolute error (MAE) [31]. Although the two metrics are similar, the RMSE penalizes outliers more. In addition, the RMSE is more similar to the OF, because it computes the square of the error. Therefore, the RMSE is chosen to be the error metric in this work. More specifically, for comparability purposes, the normalized RMSE (NRMSE) is used [32]. In this study, the error metric is given by the Equations 5.1.

$$\begin{cases} (NRMSE)_P = \dfrac{\sqrt{\frac{1}{N}\sum_{i=1}^{N}(P_{i,agg} - P_{i,det})^2}}{\frac{1}{N}\sum_{i=1}^{N} P_{i,det}} \\ (NRMSE)_Q = \dfrac{\sqrt{\frac{1}{N}\sum_{i=1}^{N}(Q_{i,agg} - Q_{i,det})^2}}{\frac{1}{N}\sum_{i=1}^{N} Q_{i,det}} \end{cases} \tag{5.1}$$

What can be considered an accurate result depends on the gaze of the observer. In this work, results with a NRMSE equal or lower to 0.03 are considered to be acceptable. Figure 5.1 illustrates an example for which the NRMSE is equal to 0.03.

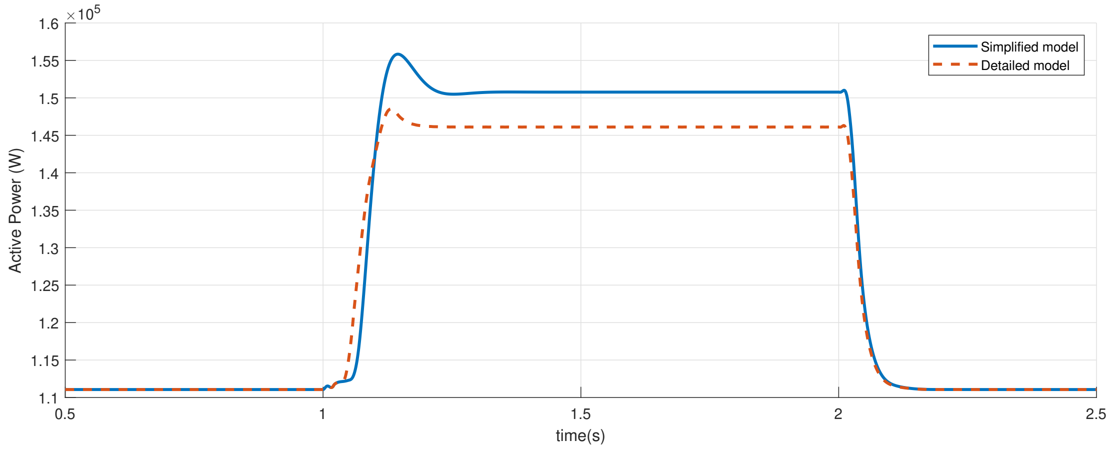

Figure 5.1: Example case for which NRMSE=0.03

5.2 Single fault training

Here, the parameter estimation is focused on optimizing the simplified model to one particular disturbance. The objective function to be minimized by the parameter estimation algorithm is simplified into the following.

$$OF = \frac{1}{N}\sum_{i=1}^{N}\Big[(P_{agg,i} - P_{det,i})^2 + (Q_{agg,i} - Q_{det,i})^2\Big] \tag{5.2}$$

For the sake of demonstration, the following faults are considered.

- Frequency deviation of $\Delta f = -3$Hz
- MV-level voltage deviation of $\Delta V_{MV} = 0.23$p.u.

Figure 5.2 depicts the objective function as a function of the algorithm evaluation number. One can observe that for both trainings, during the first iterations, it is reduced the most. After less than 200 iterations, minimum possible OF is reached. The identified parameters are respectively given in Appendix B.1 and B.2.

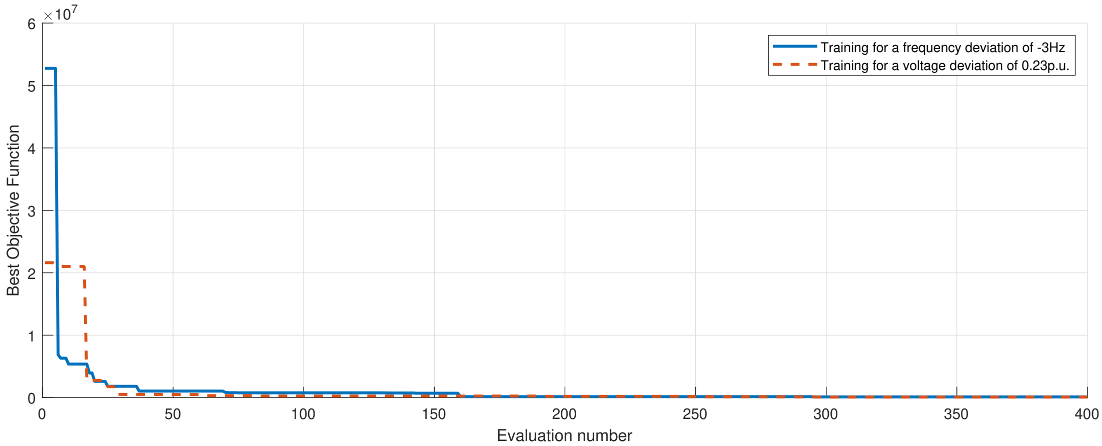

Figure 5.2: Objective Function evaluation during parameter estimation process

5.2.1 Frequency deviation of $\Delta f = -3$Hz

Figure 5.3 and 5.4 illustrate the active and reactive power respectively for a -3Hz fault. One can observe an increase in active power during the fault. This is due to the tripping of some DGs. To compensate for the missing active power generation from the tripped DGs, there is more active power coming from the grid to feed the loads. The main difference between the two model responses, is the large active power ripple during the transient. To understand the cause of the ripple, it is necessary to look at the difference between the models in terms of tripping logic. Figure 5.5 depicts the proportion of connected DGs for frequency deviations. One can observe that both models have the same amount of connected DGs for $\Delta f = -3$Hz, i.e. about 57%. However, the frequency has to be correctly measured. Figure 5.6 depicts the frequency measurement as a function of the time for the simplified model. One can see that the measurement falls below 47Hz during transient. This is the cause of the ripple, as when the frequency falls below 47Hz, the simplified model trips more generation than the detailed one. The NRMSE evaluated in the dynamic range is given in Table 5.1.

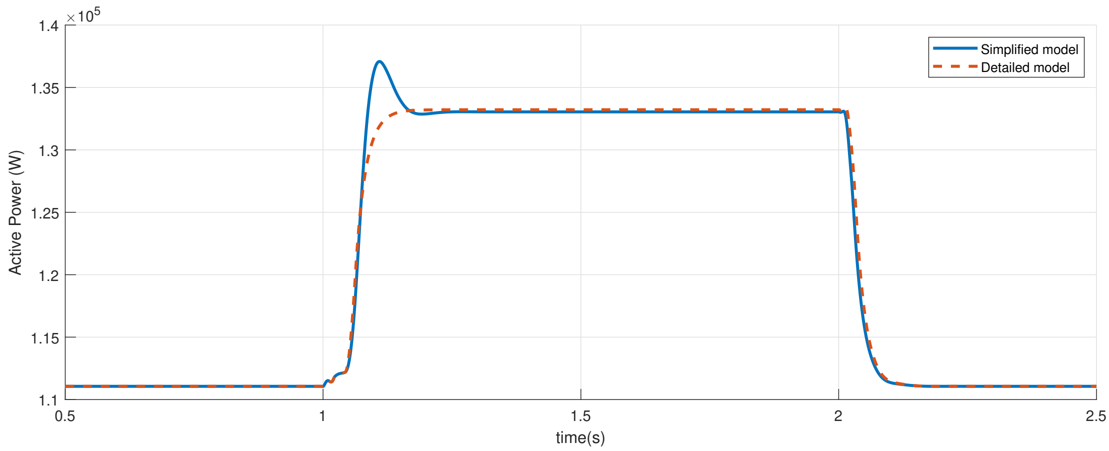

Figure 5.3: Active power for a -3Hz frequency deviation from 1s to 2s

Table 5.1: NRMSE for single fault training: -3Hz

	NRMSE
Active power	$6.7 \cdot 10^{-3}$
Reactive power	$1.1 \cdot 10^{-3}$

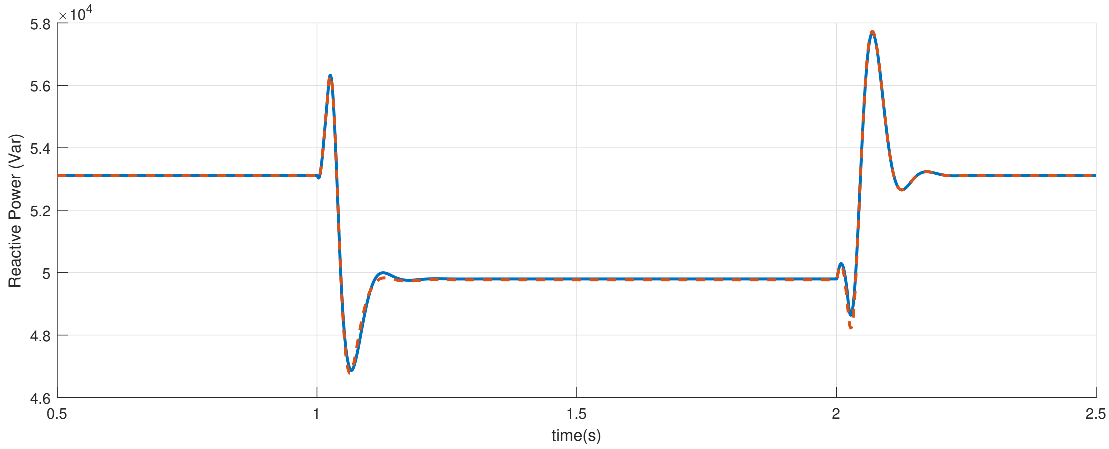

Figure 5.4: Reactive power for a -3Hz frequency deviation from 1s to 2s

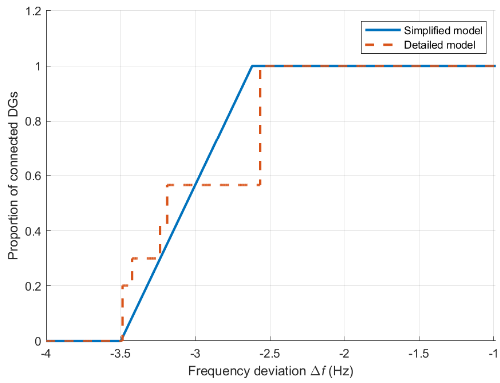

Figure 5.5: Under-frequency tripping logic due to frequency deviations

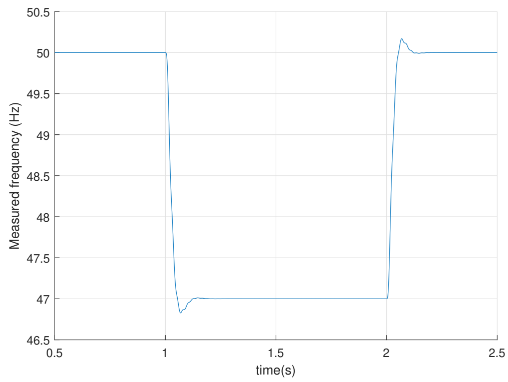

Figure 5.6: Simplified model frequency measurement for a -3Hz fault

5.2.2 MV-level voltage deviation of $\Delta V_{MV} = 0.23$p.u.

Figure 5.7 and 5.8 depict the active and reactive power respectively for 0.23p.u. fault. Due to the tripping of some DGs, there is an active power increase. The simplified model fits perfectly with the detailed one. Table 5.2 gives the NRMSE.

Table 5.2: NRMSE for single fault training: +0.23p.u.

	NRMSE
Active power	$1.4 \cdot 10^{-3}$
Reactive power	$6.6 \cdot 10^{-4}$

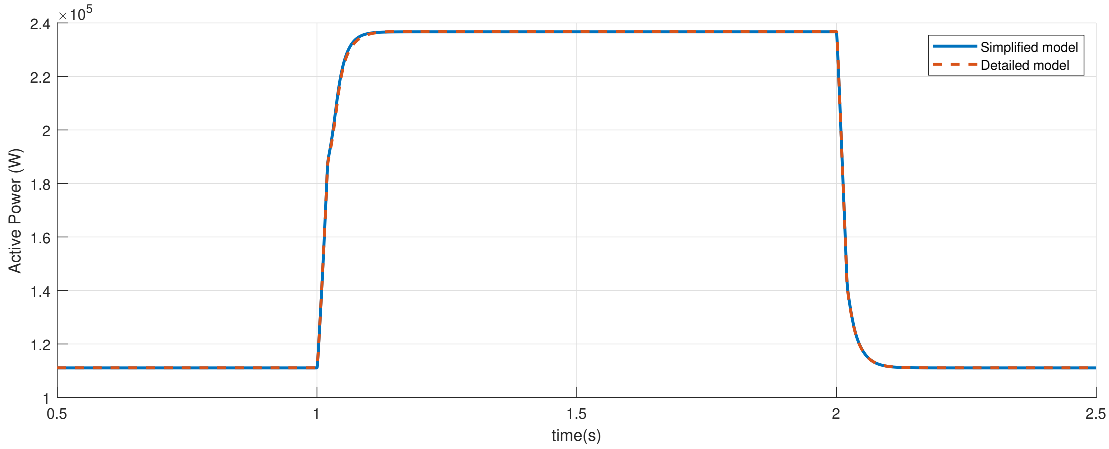

Figure 5.7: Active power for a 0.23p.u. voltage deviation from 1s to 2s

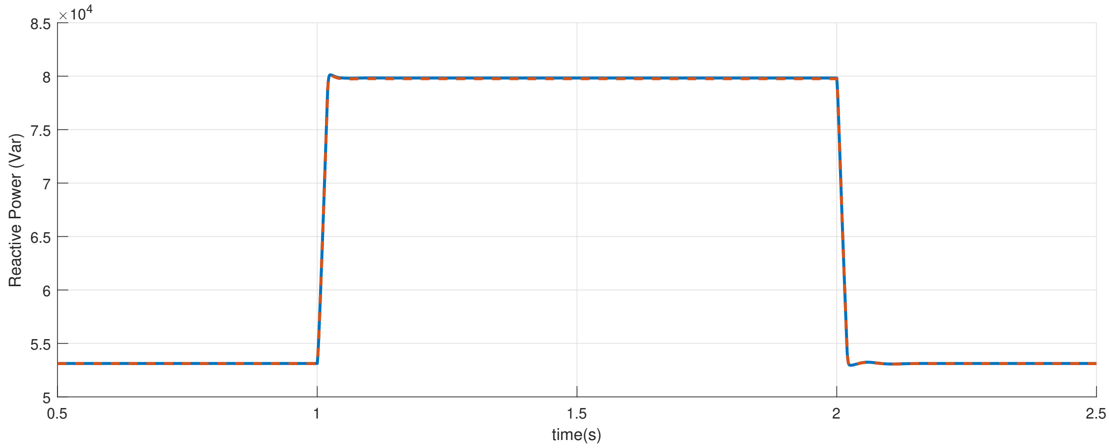

Figure 5.8: Reactive power for a 0.23p.u. voltage deviation from 1s to 2s

5.3 Training for several faults

The user may choose to train the model parameters for a specific disturbance like it has been done in the previous section, but it would be preferable for the model to be able to mimic the original model for a variety of disturbances. Ideally, all of them. In this section, the goal is to train the model for all possible frequency or voltage faults.

5.3.1 Definition of the disturbance set

The definition of a set of disturbances is required for the parameter estimation algorithm. There are a few scenarios for which the simplified and detailed model behave (almost) identically, independently of the simplified model estimated parameters.

Frequency deviations

- $\Delta f \in]-2.5\text{Hz}; 0.2\text{Hz}[$

In this range, there is neither tripping of generators nor the activation of the LFSM-O. In fact, DGs are required to stay connected for a system frequency included in [47.5Hz; 51.5Hz] and the LFSM-O is only activated starting at 50.2Hz. The active and reactive power flow of the simplified model is only a function of the equivalent line impedance $\overline{Z_{equ,line}}$, equivalent load $\overline{Z_{equ,load}}$ and equivalent power generation amount $P_{equ,DG}$.

- $\Delta f < -3.5\text{Hz}$ or $\Delta f > +2.5\text{Hz}$

For those large under and over-frequency deviations, all DGs have tripped. Both models behave the same.

Voltage deviations

If the terminal voltage V_t at each of the DGs is either below $V_{t1,min} = 0.88$p.u. or above $V_{t2,max} = 1.20$p.u., then the whole generation is disconnected. If the terminal voltage of each DG $V_t \in]V_{t1,max} = 0.90; V_{t2,min} = 1.10[$, then the whole generation is connected. Those situations are not straightforward to translate into a system disturbance, as the terminal voltage at each DG is slightly different. This is due to the different location of the DGs in the network. Figure 5.9 depicts the terminal voltage of each DG in function of the MV-level voltage. One can observe the following:

- $\Delta V_{MV} < -0.09$p.u. or $\Delta V_{MV} > +0.27$p.u.

There is full tripping in this range.

- $-0.06 < \Delta V_{MV} < +0.14$p.u.

There is no tripping at all in this range.

Conclusion

One can define the set of the above four listed cases as the set $\mathcal{A}$. It is useless to put those cases in the disturbance set, as they will not help the parameter estimation algorithm find the correct value for the simplified model parameters. On the other hand, the complement set $\mathcal{A}^c$ contains all the disturbances which depend on the simplified model parameters. This means disturbances for which there is either partial tripping and/or has the LFSM-O activated. These cases are listed below.

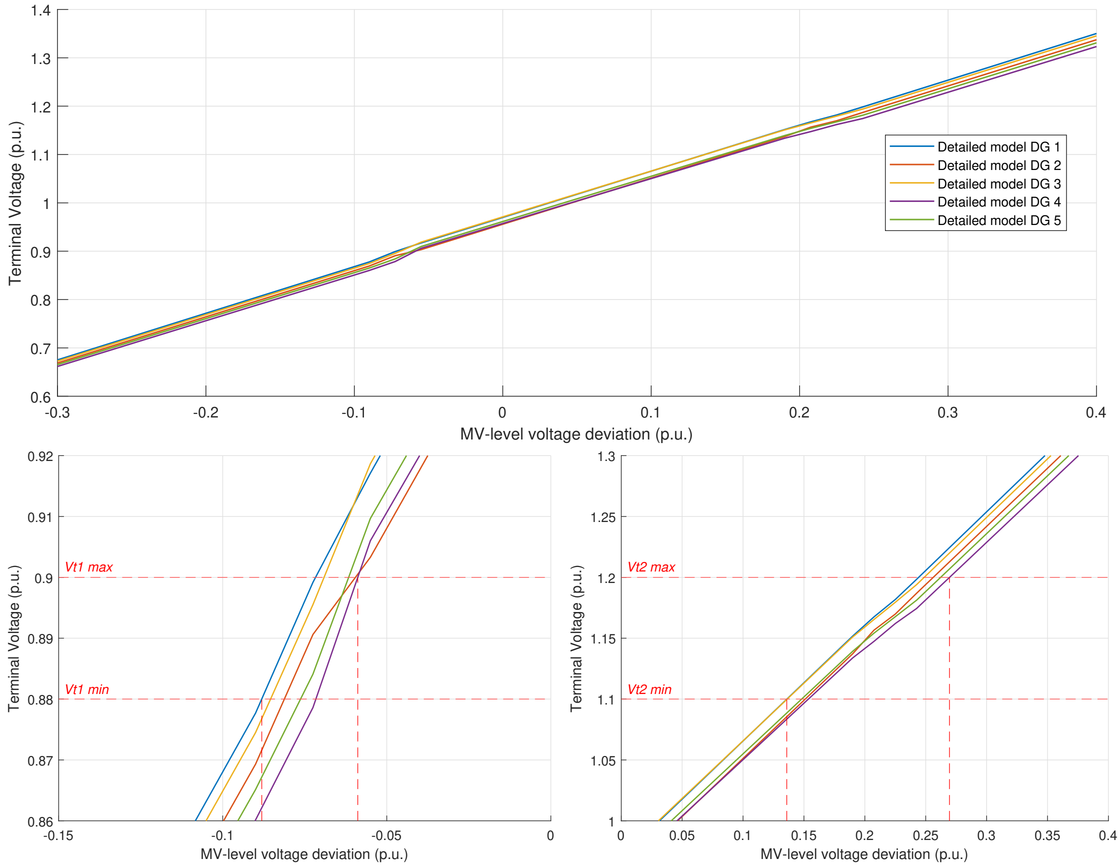

Figure 5.9: DG terminal voltage in function of MV-level voltage deviation

- $\Delta f \in [-3.5\text{Hz}; -2.5\text{Hz}]$
- $\Delta f \in [+0.2\text{Hz}; +2.5\text{Hz}]$
- $\Delta V_{MV} \in [-0.09\text{p.u.}; -0.06\text{p.u.}]$
- $\Delta V_{MV} \in [+0.14\text{p.u.}; +0.27\text{p.u.}]$

Since the disturbance set has to be finite, 25 equidistant disturbance values have been picked from each of the above cases. The disturance set is therefore of length of 100.

5.3.2 Results

The objective function as a function of the parameter estimation algorithm iteration number is depicted in Figure 5.10. One can observe that during the first iterations, the algorithm has the highest productivity. Indeed, the OF has already dropped by 88% reaching the 25^{th} evaluation. This could easily be expected. In fact, as the starting parameters are completely random and thus most probably wrong, it is easy to find ones that perform better in terms of fitness. For the next evaluations, it is harder to find new parameter values reducing the OF, so it takes more trial and errors. The identified parameters are given in Appendix B.3.

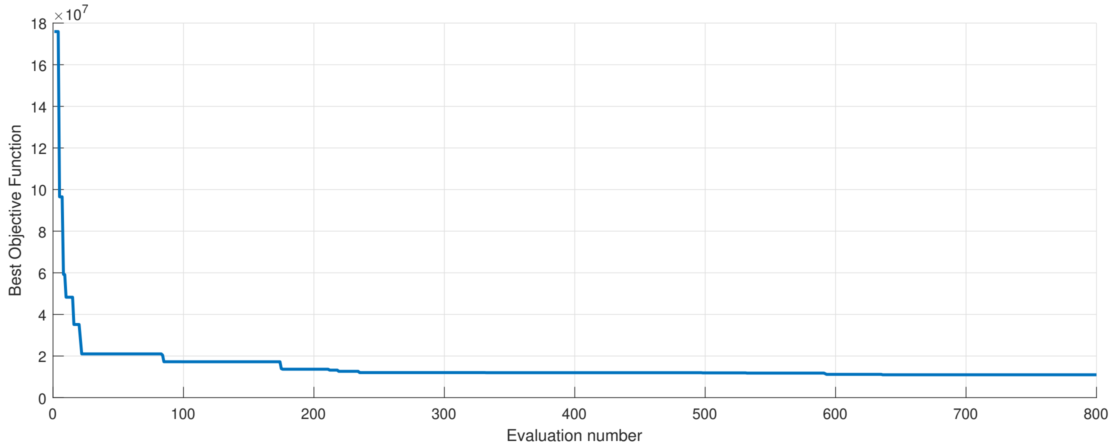

Figure 5.10: Objective Function evaluation during parameter estimation process

Analysis with respect to frequency deviations

The NRMSE as a function of the frequency deviation is depicted in Figure 5.11. Several observations can be made.

Firstly, one can see that NRMSE of the reactive power Q is zero or very close to zero. This is due to the fact that the DGs operate at a power factor of 1, so errors due to the aggregation of DGs are mainly translated into active power differences. Another observation is that the reactive power error is not zero when the active power error is not zero either. An assumption for the cause of this is that since the frequency disturbance makes the DG partially trip, the distributed active power generation loss makes the voltage slightly decrease. The load's reactive power demand is proportional to the square of the voltage (see Equation 2.7). So, if there's an active power error, there's also a reactive power error due to the difference in voltage.

Then, as expected, the NRMSE of the active power P is zero for $\Delta f \in]-2.5\text{Hz}; 0.2\text{Hz}[$ for the reasons discussed in Section 5.3.1. The worst accuracy is achieved in the under-frequency partial tripping interval, i.e. for $\Delta f \in [-3.5\text{Hz}; -2.5\text{Hz}]$. To understand that, the generator tripping profile due to frequency deviations of the detailed and simplified model is depicted in Figure 5.12.

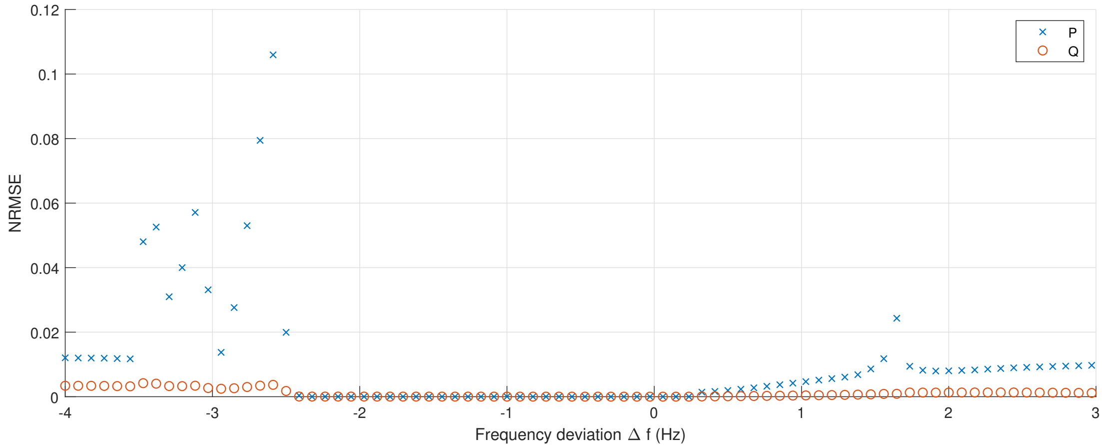

Figure 5.11: NRMSE for frequency deviations

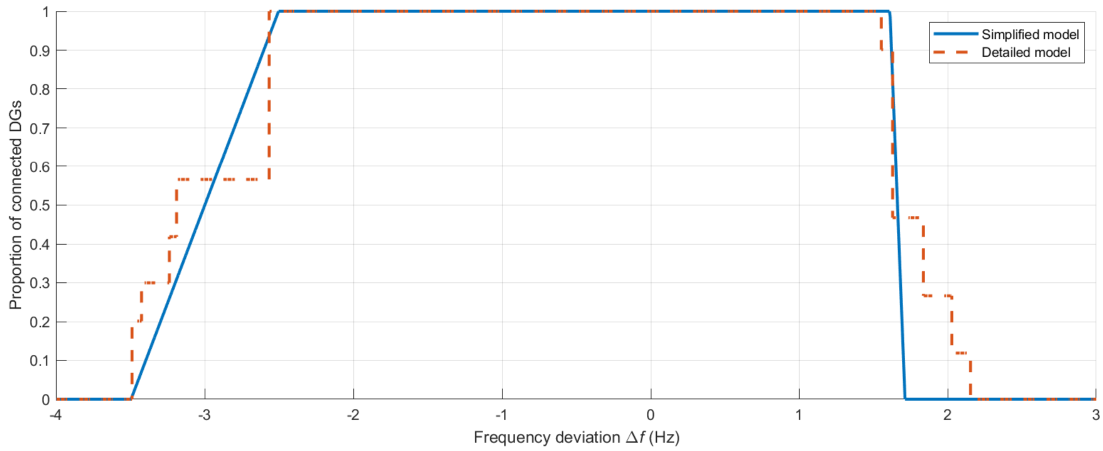

Figure 5.12: Tripping logic due to frequency deviations

In order to find a correlation between the tripping profile and the NRMSE, the absolute value of the difference between detailed and simplified model tripping profile is computed and plotted together with the active power NRMSE in Figure 5.13. One can observe that there is indeed a correlation between partial tripping error and the active power NRMSE for $\Delta f \in [-3.5\text{Hz}; -2.5\text{Hz}]$. However, for $\Delta f \in [+0.2\text{Hz}; +2.5\text{Hz}]$ one has in addition to the partial tripping, also to take into account the fact that there is the LFSM-O.

Figure 5.14 illustrates the active power reduction due to the LFSM-O. One can observe that both models behave identically, so the error for $\Delta f \in [+0.2\text{Hz}; +2.5\text{Hz}]$ is not related to the bad estimation of the down regulation droop Ddn.

Therefore, an assumption is that the active power NRMSE for $\Delta f \in [+0.2\text{Hz}; +2.5\text{Hz}]$ is lower than in $[-3.5\text{Hz}; -2.5\text{Hz}]$, because the algorithm not only benefited of the

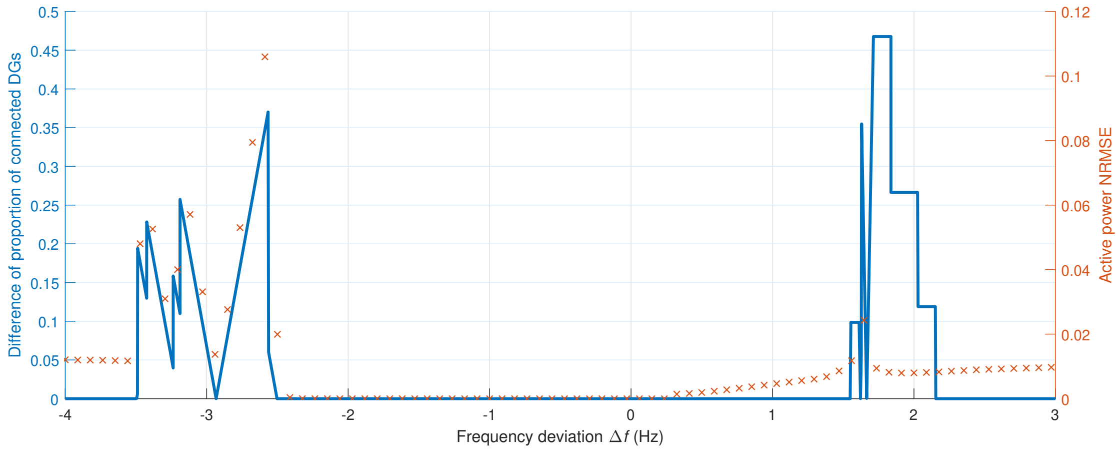

Figure 5.13: Absolute value of difference of tripping logic and active power NRMSE for frequency deviations

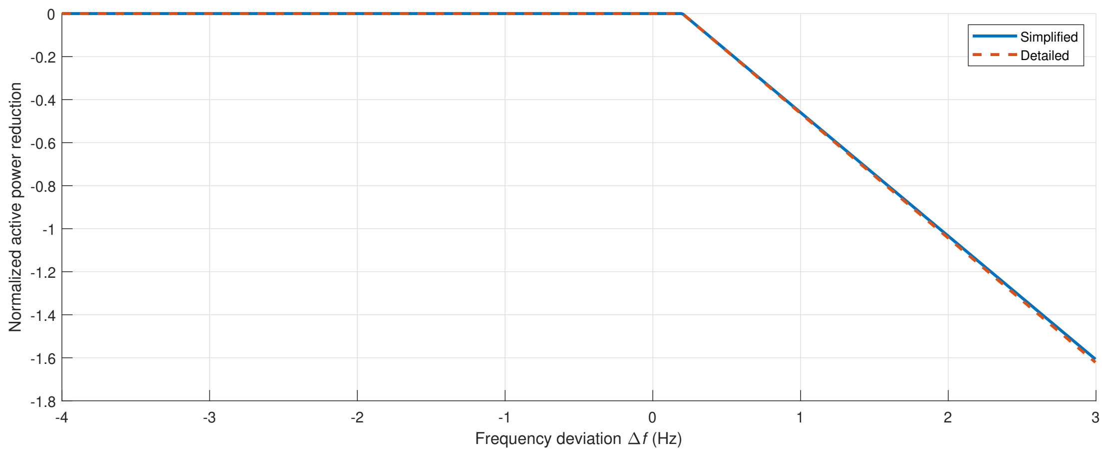

Figure 5.14: Normalized active power reduction due to the LFSM-O

over-frequency partial tripping parameters, but also of the down-regulation droop parameter due to the LFSM-O to minimize the error. To support this assumption, both models normalized active power output command is measured for all the considered frequency disturbances and depicted in Figure 5.15.

The difference between the two curves in Figure 5.15 is computed and plotted together with the active power NRMSE in Figure 5.16. One can observe a clear correlation.

Finally, concerning the case where all the generators have tripped in both models, i.e. for $\Delta f < -3.5$Hz or $\Delta f > +1.5$Hz, there is a non-zero NRMSE. This is due to the difference in time it takes for the whole generation to trip or to reconnect as depicted in Figure 5.17, because of the difference in frequency

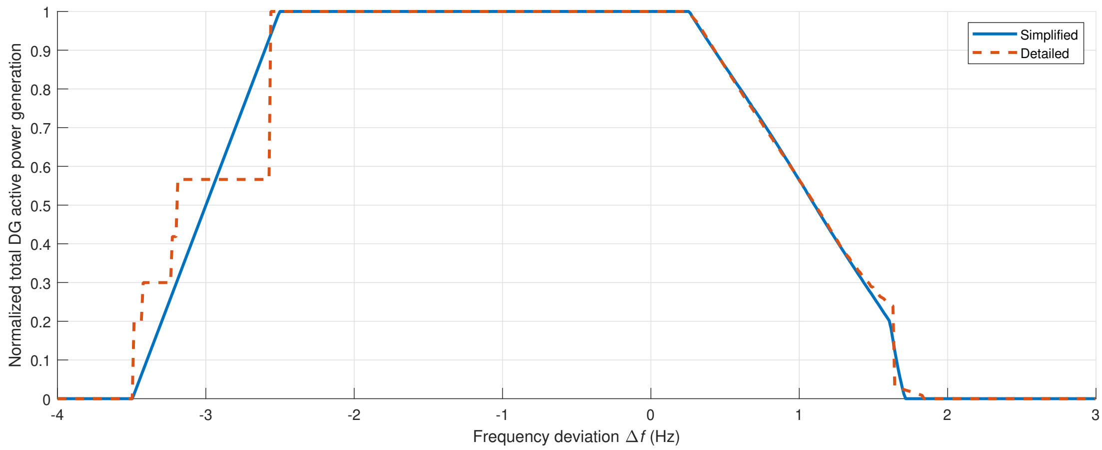

Figure 5.15: Normalized active power ouput

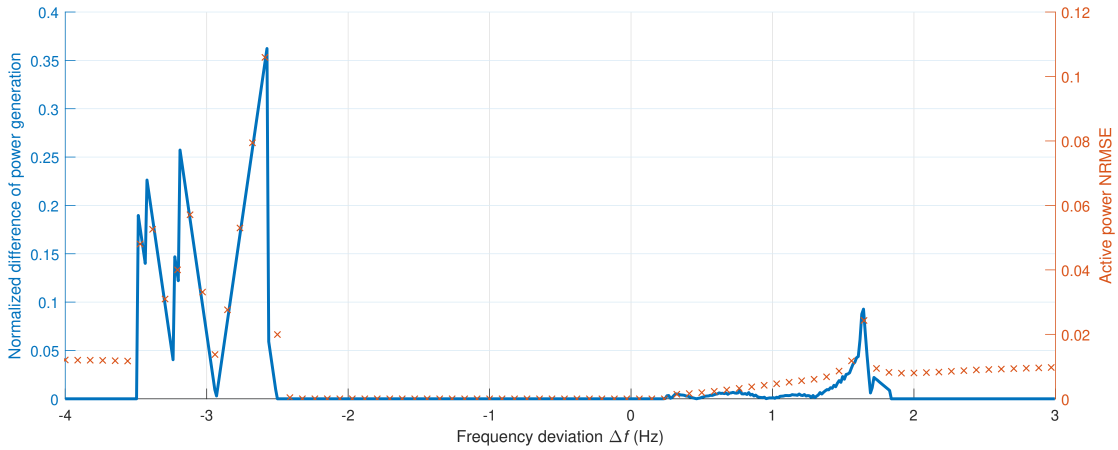

Figure 5.16: Absolute value of difference of active power output and active NRMSE for frequency deviations

measurement response (This is not only the case for $\Delta f < -3.5$Hz or $\Delta f > +1.5$Hz but everywhere where the active power NRMSE$\neq 0$). More specifically, the error due to the PLL parameters $k_{p,PLL}$, $k_{i,PLL}$ and w_c. That phenomena can be observed in Figure 5.18, where frequency measurements are depicted for a +2.5Hz fault.

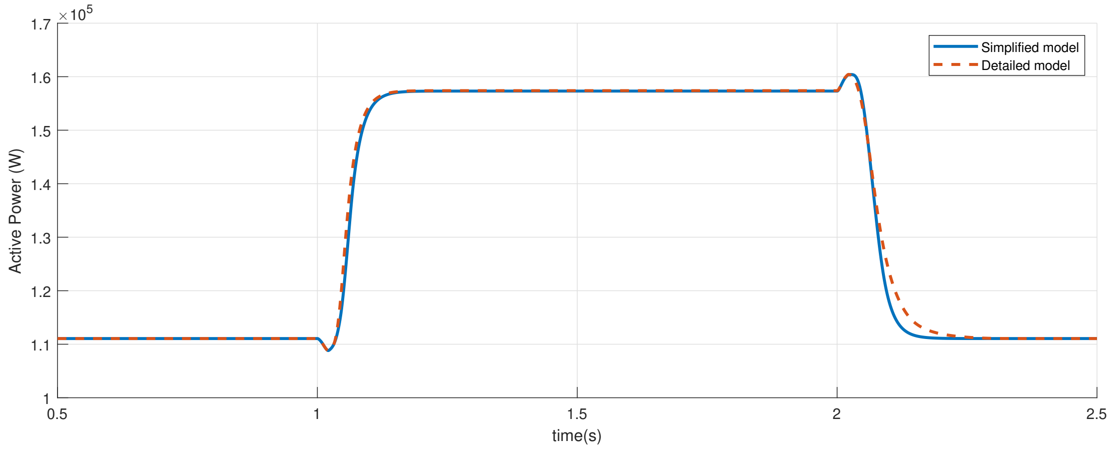

Figure 5.17: Active power for a +2.5Hz frequency deviation from 1s to 2s

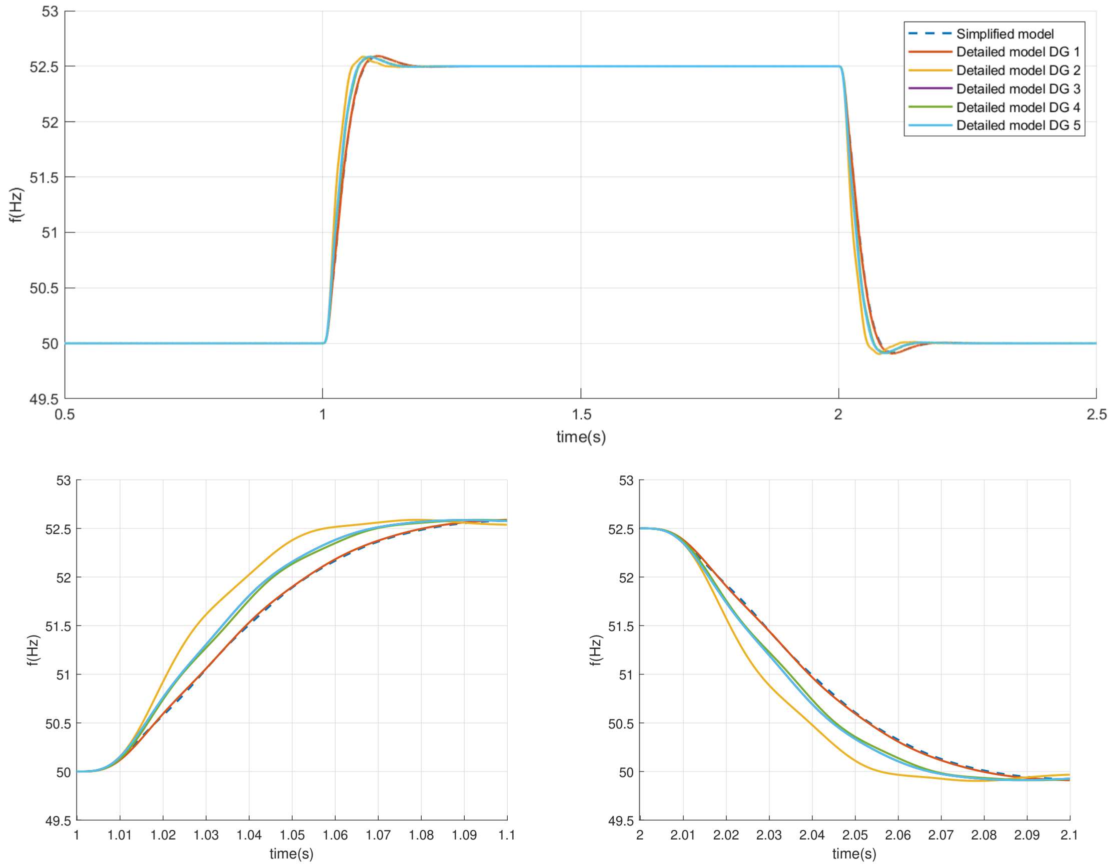

Figure 5.18: Frequency measurements for a +2.5Hz deviation from 1s to 2s

Analysis with respect to voltage deviations

Figure 5.19 depicts the NRMSE for MV-level voltage faults of different magnitude. Like expected, the NRMSE is non-zero in the range where there is partial tripping. Figure 5.20 depicts the proportion of connected DGs for both models as a function of the MV-level voltage. In order to verify if there is a correlation, the absolute value of the difference of the proportion of connected DGs is computed and plotted together with the active power NRMSE in Figure 5.21. One can observe that indeed the two correlate.

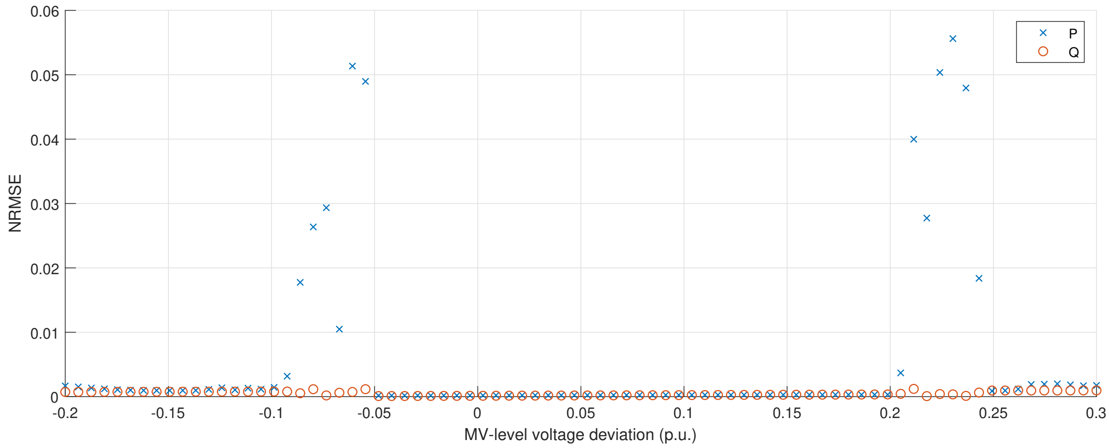

Figure 5.19: NRMSE for voltage deviations

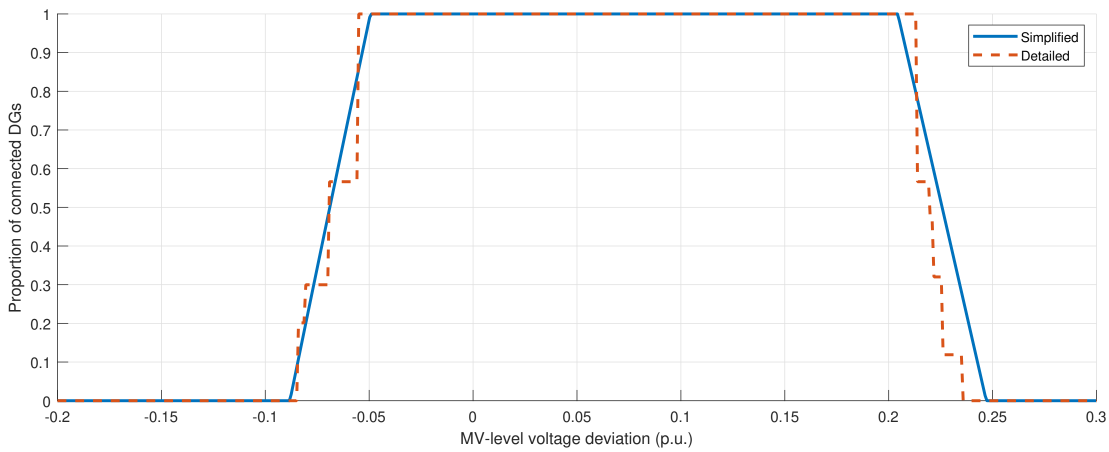

Figure 5.20: Tripping logic due to MV-level voltage deviations

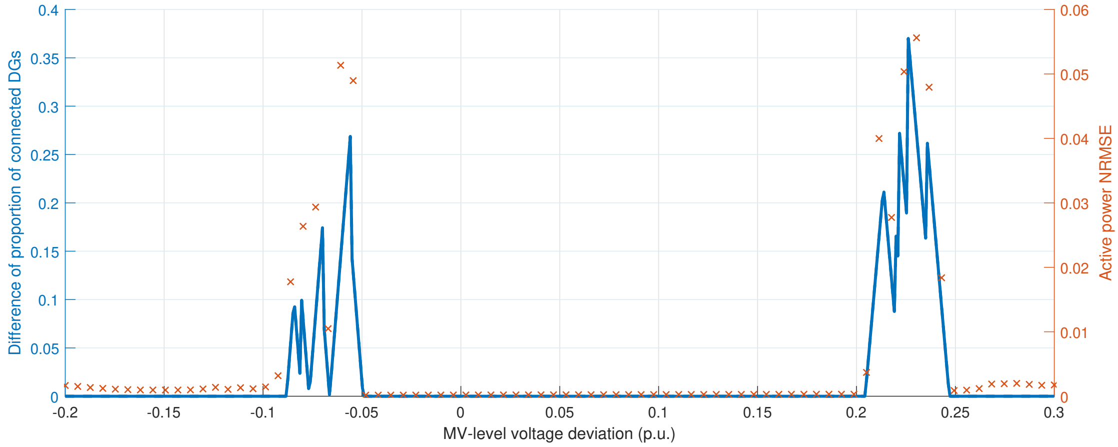

Figure 5.21: Absolute value of difference of tripping logic and active power NRMSE for MV-level voltage deviations

Conclusion on the accuracy

For the considered disturbances, the NRMSE is generally less than 0.012 except for the cases where there is partial tripping. For the disturbances with partial tripping, the NRMSE occasionally exceeds the limit of acceptability of 0.03. To conclude, partial tripping is the main limiting factor in the accuracy of the equivalent model.

5.4 Increasing complexity

Now, the question is whether the methodology for creating the reduced-order model can be extended to a more complex network while maintaining reasonable accuracy. To investigate this, the detailed model complexity is increased by extending the number of lines and DGs. Figure 5.22 and Figure 5.23 illustrate the two considered test cases. In the first network, the number of lines, loads and DGs have been increased by 2 and in the second by 3. The transformer rating has been changed accordingly. To be more concise, the 5 lines, 5 loads and 5 DGs case is referred to as a complexity level of 5. The same denomination logic is used for the 10 lines, 10 loads, 10 DGs and for the 15 lines, 15 loads and 15 DGs case. It is important to mention that the size of the disturbance set used by the parameter identification algorithm has been decreased here from 100 to 60. This has been done to reduce the parameter identification time. Appendix A.2 and A.3 give the network parameters for the complexity level 10 and 15 respectively. Appendix B.3.2 and B.3.3 give the parameter identification results.

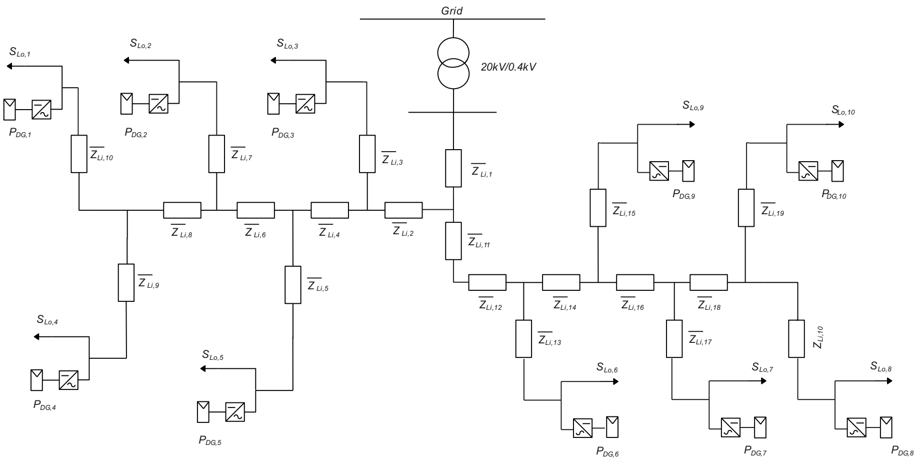

Figure 5.22: Benchmark network of complexity level 10

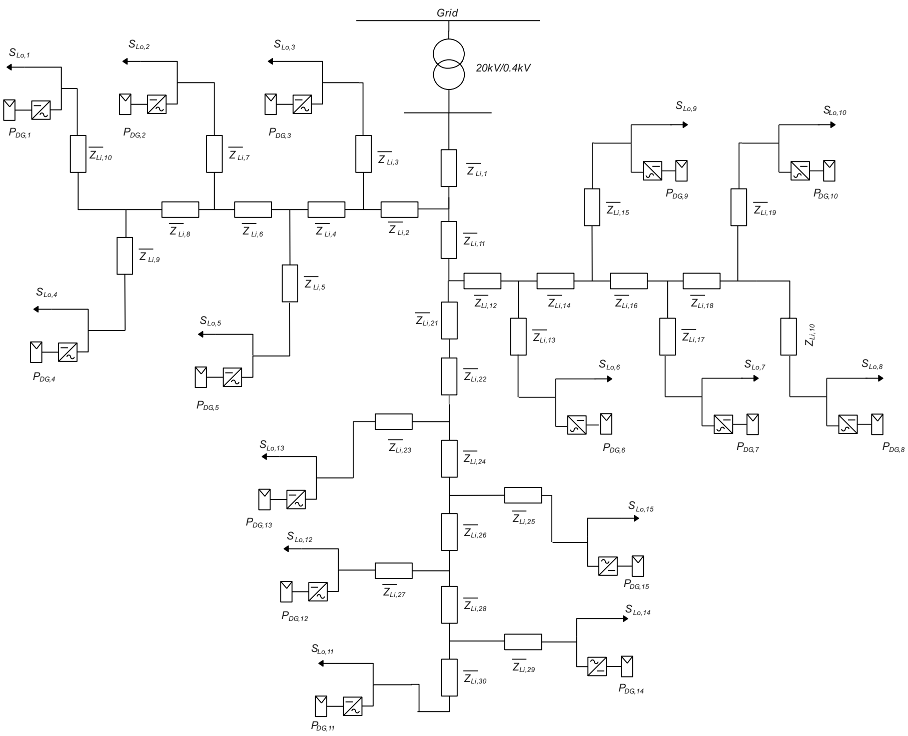

Figure 5.23: Benchmark network of complexity level 15

5.4.1 Overview of accuracy

The NRMSE distribution for the different complexity levels is compared in this subsection. A proper manner to illustrate error distributions is to use box plots. However, due to the comparatively larger errors for the disturbances where there is partial tripping, there would be a high number of outliers. This would make the distribution analysis difficult. Alternatively, violin plots show the distribution in a simpler way.

Violin plots of the active and reactive power NRMSE distribution for the frequency disturbances and for voltage disturbances are shown in Figures 5.24 and 5.25 respectively. Frequency deviations used for the datasets range from -3Hz to 4Hz, equally spaced. For voltage deviations, the datasets range from -0.2 p.u. to 0.3 p.u. equally spaced. Each dataset is of size 80.

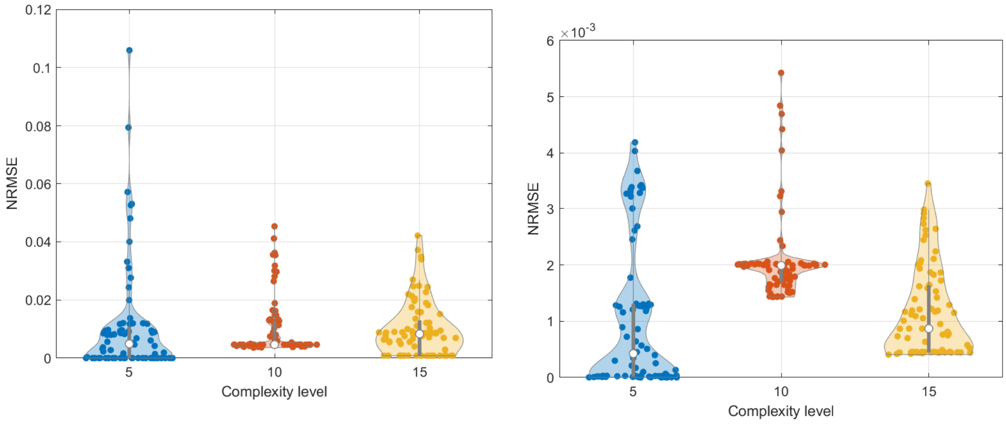

Figure 5.24: Violin plots for frequency deviations for active power (left) and reactive power (right)

The first observation is that for the reactive power, even if the error is slightly higher for the increased complexity levels, it is still negligibly small. Concerning the active power, the NRMSE has remained in a relatively similar order of magnitude when increasing the complexity level. However, for the active power errors in the case of voltage deviations, the maximum NRMSE has increased with the complexity level. This could be due to the tripping parameters (due to voltage deviation) that are distributed in a manner that the linear partial tripping cannot approximate correctly. Another assumption is that the parameter identification algorithm has been stopped too early.

Globally, the NRMSE has remained in a reasonable range, so the equivalent model is valid for more complex networks.

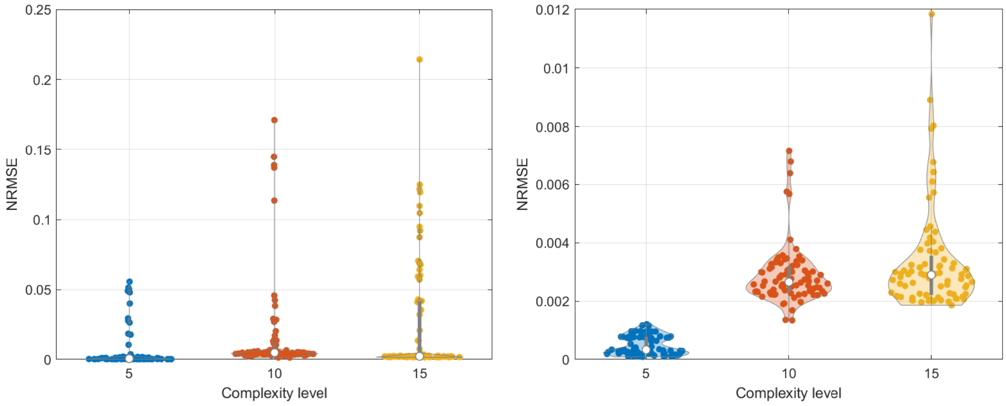

Figure 5.25: Violin plots for voltage deviations for active power (left) and reactive power (right)

5.4.2 Time savings of the simulation

The time savings for using the reduced-order model are assessed by measuring the simulation time of both models for several faults. For this purpose, the amount of logged data is minimized. Only the active and reactive power at the PCC are stored. The simulations were carried out on an Intel Core i7-7700HQ CPU with 32 GB RAM. The three cases with different complexity are considered for different faults and compared to the equivalent model. Table 5.3 show the mean simulations time measurements and the mean time reduction for the 5, 10 and 15 complexity levels respectively. The complete data used for Table 5.3 is given in Appendix C.

	Simulation time (s)		Comparison	
Complexity level	Detailed model	Reduced-order model	Difference (s)	Reduction (%)
5	21.34	4.61	17.27	**78.4**
10	45.55	4.19	41.36	**90.8**
15	68.63	4.38	64.25	**93.6**

Table 5.3: Mean simulation time comparison for different complexity levels

One observes that for a network with an increased complexity, the simulation time is increased as well. Meanwhile, the reduced-order model simulation time remains in the same order of magnitude. Therefore, the interest, i.e. the simulation time gains using the reduced-order model is higher for larger networks with more DGs.

Chapter 6

Conclusion

Summary

In this thesis, a benchmark distribution network containing distributed generators (DGs) and loads with a power factor of 0.95 has been used. The lines, loads and DGs models have been described. The DG model functionalities like the tripping of the generator for protection and the limited frequency sensitivity mode for over frequency have been explained. The methodology to create an equivalent model based on the grey box approach has been described. To find the equivalent model parameters, the Mean-Variance Mapping Optimization algorithm has been used. The algorithm operation has been stated and the algorithm initialization parameters choice has been discussed. Then, the equivalent model accuracy has been assessed. The main contribution of this thesis has been the analysis of the accuracy of the investigated equivalent model. The main results were the following:

- When the model is trained for a single disturbance, the model is perfectly able to mimic the original from the point of view of power flow at the point of common coupling.
- When the model is trained for several disturbances, it has good accuracy, except for some cases when there is partial tripping of generators.
- It has also been established that the equivalent model of a network containing more lines, loads and DGs is still able to achieve good accuracy.
- To use the equivalent model makes the user significantly save simulation time. For example, for the 15 lines, loads and DGs the equivalent model simulation runs 93.6% faster than the original model.

Directions for future work

Globally, the main drawback of the equivalent model is related to the partial tripping. To find a better alternative to the applied linear partial tripping would constitute an interesting improvement of the model. More ways how this project could be extended are the following:

- Add some parameters to be determined by the parameter identification algorithm. In particular, the power provided by the aggregated DG has been computed as the sum of the power of all DGs. Instead, this quantity could have been determined by the parameter identification algorithm. This could possibly increase the accuracy. With the same reasoning, the aggregated load value could be a parameter to be identified.

- To use a more realistic model for the distributed generator in the detailed model. In fact, normally, solar photovoltaic generators in distribution networks are connected to a single line. The accuracy analysis would indicate if the equivalent model is valid in this case or if modifications of the model are needed.

- Only solar photovoltaic generators have been considered in this work. The equivalent model is nevertheless supposed to be able to take into account the behaviour of other DGs such as wind turbines or combined heat and power systems. It would be interesting to validate the model for this generators.

- This model works for a balanced network with balanced three-phase faults. A model that would also accurately mimic a system under unbalanced conditions would be a significant improvement.

- A reduced-order model of a LV network has been created and validated. Whether it is possible to extend the methodology for the creation of an accurate equivalent model of a MV network would be interesting.

Bibliography

[1] EUI. (2022, December) Renewable energy in the european union. [Online]. Available: https://fsr.eui.eu/renewable-energy-in-the-european-union/

[2] EMBER. (2022, December) Eu power sector in 2020. [Online]. Available: https://ember-climate.org/insights/research/eu-power-sector-2020/

[3] Z. Science. (2022, December) Environment, news, renewable energy, science. [Online]. Available: https://www.zmescience.com/science/news-science/eu-bets-on-solar-power-to-cut-its-reliance-on-russias-natural-gas-19052022/

[4] G. Intégration. (2022, December) Residential solar roofs graowing strongly in belgium. [Online]. Available: https://www.gseintegration.com/en/2021/06/19/residential-solar-roofs-growing-strongly-in-belgium/

[5] Eurostat. Electrical capacity for wind and solar photovoltaic power - statistics. [Online]. Available: https://ec.europa.eu/eurostat/statistics-explained/, year = 2022, month=December,

[6] C.-C. J. W. G. C4/C6.35, *MODELLING OF INVERTER-BASED GENERATION FOR POWER SYSTEM DYNAMIC STUDIES*, 2018.

[7] M. Reza, M. Gibescu, P. H. Schavemaker, W. L. Kling, and L. van der Sluis, "Transient stability impacts of a 'vertical-to-horizontal' transformation of power systems," 2005. [Online]. Available: https://ieeexplore.ieee.org/document/4524661?arnumber=4524661

[8] F. O. Resende, J. Matevosyan, and J. V. Milanovic, "Application of dynamic equivalence techniques to derive aggregated models of active distribution network cells and microgrids," 2013. [Online]. Available: https://ieeexplore-ieee-org.proxy.bib.uclouvain.be:2443/document/6652356

[9] E. O. Kontis, S. P. Dimitrakopoulos, A. I. Chrysochos, G. K. Papagiannis, and T. A. Papadopoulos, "Dynamic equivalencing of active distribution grids," pp. 1–6, 2017.

[10] G. San, W. Zhang, X. Guo, C. Hua, H. Xin, and F. Blaabjerg, "Large-disturbance stability for power-converter-dominated microgrid: A review," *Renewable and Sustainable Energy Reviews*, vol. 127, p. 109859, 2020. [Online]. Available: https://www.sciencedirect.com/science/article/pii/S1364032120301532

[11] G. Chaspierre, P. Panciatici, and T. Van Cutsem, "Dynamic equivalent of a distribution grid hosting dispersed photovoltaic units," 2017. [Online]. Available: http://irep2017.inesctec.pt/conference-papers

[12] G. Chaspierre, "Reduced-order modelling of active distribution networks for large-disturbance simulations," Ph.D. dissertation, ULiège - Université de Liège, 14 December 2020.

[13] M. Wajahat, H. A. Khalid, G. M. Bhutto, and C. Leth Bak, "A comparative study into enhancing the pv penetration limit of a lv cigre residential network with distributed grid-tied single-phase pv systems," *Energies*, vol. 12, no. 15, 2019. [Online]. Available: https://www.mdpi.com/1996-1073/12/15/2964

[14] MathWorks. (2022, December) Three-phase series rlc load. [Online]. Available: https://nl.mathworks.com/help/sps/powersys/ref/threephaseseriesrlcload.html

[15] ——. (2022, December) Three-phase series rlc branch. [Online]. Available: https://nl.mathworks.com/help/sps/powersys/ref/threephaseseriesrlcbranch.html

[16] H. Alenius, R. Luhtala, T. Messo, and T. Roinila, "Autonomous reactive power support for smart photovoltaic inverter based on real-time grid-impedance measurements of a weak grid," *Electric Power Systems Research*, vol. 182, p. 106207, 2020. [Online]. Available: https://www.sciencedirect.com/science/article/pii/S0378779620300146

[17] Elia, *PROPOSAL FOR NC RFG REQUIREMENTS OF GENERAL APPLICATION*, 2018.

[18] C. Rogiest, "Modelling active distribution grids in power systems frequency stability studies," 2022.

[19] Entsoe, *Limited frequency sensitive mode, ENTSO-E guidance document for national implementation for network codes on grid connection*, 2018.

[20] D. Luengo, L. Martino, M. Bugallo, V. Elvira, and S. Särkkä, "A survey of monte carlo methods for parameter estimation," *EURASIP Journal on Advances in Signal Processing*, vol. 2020, 05 2020.

[21] J. Yang, J. Zhang, and W. Pan, "Dynamic equivalents of power system based on extended two particle swarm optimization," vol. 5, pp. 609–613, 2007.

[22] V. Miranda and R. Alves, "Differential evolutionary particle swarm optimization (deepso): A successful hybrid," pp. 368–374, 2013.

[23] D. Gusain, J. L. Rueda, J. C. Boemer, and P. Palensky, "Identification of dynamic equivalents of active distribution networks through mvmo," *IFAC-PapersOnLine*, vol. 49, no. 27, pp. 262–267, 2016, iFAC Workshop on Control of Transmission and Distribution Smart Grids CTDSG 2016. [Online]. Available: https://www.sciencedirect.com/science/article/pii/S2405896316323205

[24] F. Bu, Z. Ma, Y. Yuan, and Z. Wang, "Wecc composite load model parameter identification using evolutionary deep reinforcement learning," *IEEE Transactions on Smart Grid*, vol. 11, no. 6, pp. 5407–5417, 2020.

[25] G. Venayagamoorthy and W. Nakawiro, "A mean-variance optimization algorithm," 2010. [Online]. Available: https://ieeexplore.ieee.org/document/5586027?arnumber=5586027

[26] A. Gbadamosi, J. L. Rueda, D. Wang, and P. Palensky, "Application of mean-variance mapping optimization for parameter identification in real-time digital simulation," in *2017 Federated Conference on Computer Science and Information Systems (FedCSIS)*, 2017, pp. 11–16.

[27] J. L. Rueda and I. Erlich, "Mvmo for bound constrained single-objective computationally expensive numerical optimization," in *2015 IEEE Congress on Evolutionary Computation (CEC)*, 2015, pp. 1011–1017.

[28] I. Erlich, J. L. Rueda, S. Wildenhues, and F. Shewarega, "Solving the ieee-cec 2014 expensive optimization test problems by using single-particle mvmo," in *2014 IEEE Congress on Evolutionary Computation (CEC)*, 2014, pp. 1084–1091.

[29] M. N. Vincent Kenny and S. Saldana. (2022, December) Heuristic algorithms. [Online]. Available: https://optimization.mccormick.northwestern.edu/index.php/Heuristic_algorithms

[30] (2022, December) Heuristics. [Online]. Available: https://www.techopedia.com/definition/5436/heuristic: :text=Heuristics

[31] (2022, December) Regression metrics for machine learning. [Online]. Available: https://machinelearningmastery.com/regression-metrics-for-machine-learning/

[32] (2022, December) Nrmse. [Online]. Available: https://www.statisticshowto.com/nrmse/

Appendix A

Detailed model parameters

A.1 Complexity level 5

Table A.1: Generated detailed model parameters complexity level 5 part 1/2

Parameter	Value	Unit	Parameter	Value	Unit
$P_{Lo,1}$	33.17	kW	$F_{t1,1}$	46.58	Hz
$P_{Lo,2}$	55.09	kW	$F_{t1,2}$	46.58	Hz
$P_{Lo,3}$	25.67	kW	$F_{t1,3}$	46.51	Hz
$P_{Lo,4}$	37.30	kW	$F_{t1,4}$	46.81	Hz
$P_{Lo,5}$	20.13	kW	$F_{t1,5}$	46.76	Hz
$Q_{Lo,1}$	10.90	kVar	$F_{t2,1}$	51.55	Hz
$Q_{Lo,2}$	18.11	kVar	$F_{t2,2}$	51.63	Hz
$Q_{Lo,3}$	8.44	kVar	$F_{t2,3}$	51.84	Hz
$Q_{Lo,4}$	12.26	kVar	$F_{t2,4}$	52.03	Hz
$Q_{Lo,5}$	6.62	kVar	$F_{t2,5}$	52.15	Hz
$P_{DG,1}$	4.99	kW	$V_{t1,1}$	0.891	p.u.
$P_{DG,2}$	21.95	kW	$V_{t1,2}$	0.891	p.u.
$P_{DG,3}$	10.18	kW	$V_{t1,3}$	0.883	p.u.
$P_{DG,4}$	7.47	kW	$V_{t1,5}$	0.894	p.u.
$P_{DG,5}$	6.02	kW	$V_{t2,5}$	1.175	p.u.
$Q_{DG,1}$	0	kVar	$V_{t2,1}$	1.178	p.u.
$Q_{DG,2}$	0	kVar	$V_{t2,2}$	1.147	p.u.
$Q_{DG,3}$	0	kVar	$V_{t2,3}$	1.179	p.u.
$Q_{DG,4}$	0	kVar	$V_{t2,4}$	1.160	p.u.
$Q_{DG,5}$	0	kVar	$V_{t2,5}$	1.175	p.u.

Table A.2: Generated detailed model parameters complexity level part 2/2

Parameter	Value	Unit	Parameter	Value	Unit
Ddn_1	0.793	$\frac{1}{Hz}\cdot$ p.u. on mbase	$k_{i,PLL,1}$	810.0	Hz
Ddn_2	0.380	$\frac{1}{Hz}\cdot$ p.u. on mbase	$k_{i,PLL,3}$	750.7	Hz
Ddn_3	0.589	$\frac{1}{Hz}\cdot$ p.u. on mbase	$k_{i,PLL,4}$	970.0	Hz
Ddn_4	0.749	$\frac{1}{Hz}\cdot$ p.u. on mbase	$k_{i,PLL,5}$	884.0	Hz
Ddn_5	0.910	$\frac{1}{Hz}\cdot$ p.u. on mbase	$F_{t1,5}$	46.76	Hz
$T_{resp,1}$	0.058	s	w_{c1}	42.46	rad/s
$T_{resp,2}$	0.033	s	w_{c2}	57.52	rad/s
$T_{resp,3}$	0.008	s	w_{c3}	49.80	rad/s
$T_{resp,4}$	0.009	s	w_{c4}	48.70	rad/s
$T_{resp,5}$	0.016	s	w_{c5}	60.23	rad/s
$k_{p,PLL,1}$	110.4	Hz			
$k_{p,PLL,2}$	75.3	Hz			
$k_{p,PLL,3}$	108.9	Hz			
$k_{p,PLL,4}$	74.6	Hz			
$k_{p,PLL,5}$	115.8	Hz			

A.2 Complexity level 10

Table A.3: Generated detailed model parameters complexity level 10 part 1/2

Parameter	Value	Unit	Parameter	Value	Unit
$P_{Lo,1}$	17.27	kW	$Q_{DG,1}$	0	kVar
$P_{Lo,2}$	41.13	kW	$Q_{DG,2}$	0	kVar
$P_{Lo,3}$	51.98	kW	$Q_{DG,3}$	0	kVar
$P_{Lo,4}$	34.04	kW	$Q_{DG,4}$	0	kVar
$P_{Lo,5}$	42.88	kW	$Q_{DG,5}$	0	kVar
$P_{Lo,6}$	16.80	kW	$Q_{DG,6}$	0	kVar
$P_{Lo,7}$	54.79	kW	$Q_{DG,7}$	0	kVar
$P_{Lo,8}$	35.19	kW	$Q_{DG,8}$	0	kVar
$P_{Lo,9}$	41.79	kW	$Q_{DG,9}$	0	kVar
$P_{Lo,10}$	11.24	kW	$Q_{DG,10}$	0	kVar
$Q_{Lo,1}$	5.68	kVar	$F_{t1,1}$	47.13	Hz
$Q_{Lo,2}$	13.52	kVar	$F_{t1,2}$	47.15	Hz
$Q_{Lo,3}$	17.09	kVar	$F_{t1,3}$	46.53	Hz.
$Q_{Lo,4}$	11.19	kVar	$F_{t1,4}$	46.87	Hz
$Q_{Lo,5}$	14.09	kVar	$F_{t1,5}$	46.68	Hz.
$Q_{Lo,6}$	5.52	kVar	$F_{t1,6}$	46.72	Hz
$Q_{Lo,7}$	18.01	kVar	$F_{t1,7}$	46.68	Hz
$Q_{Lo,8}$	11.57	kVar	$F_{t1,8}$	47.16	Hz
$Q_{Lo,9}$	13.74	kVar	$F_{t1,9}$	47.41	Hz
$Q_{Lo,10}$	3.69	kVar	$F_{t1,10}$	46.88	Hz
$P_{DG,1}$	8.52	kW	$F_{t2,1}$	51.85	Hz
$P_{DG,2}$	18.09	kW	$F_{t2,2}$	52.11	Hz
$P_{DG,3}$	18.11	kW	$F_{t2,3}$	51.92	Hz
$P_{DG,4}$	9.89	kW	$F_{t2,4}$	52.34	Hz
$P_{DG,5}$	9.16	kW	$F_{t2,5}$	52.46	Hz
$P_{DG,6}$	7.09	kW	$F_{t2,6}$	51.87	Hz
$P_{DG,7}$	11.04	kW	$F_{t2,7}$	51.55	Hz
$P_{DG,8}$	4.66	kW	$F_{t2,8}$	51.88	Hz
$P_{DG,9}$	17.90	kW	$F_{t2,9}$	52.30	Hz
$P_{DG,10}$	4.36	kW	$F_{t2,10}$	52.12	Hz

Table A.4: Generated detailed model parameters complexity level 10 part 2/2

Parameter	Value	Unit	Parameter	Value	Unit
$V_{t1,1}$	0.900	p.u.	$T_{resp,6}$	0.029	s
$V_{t1,2}$	0.888	p.u.	$T_{resp,7}$	0.046	s
$V_{t1,3}$	0.884	p.u.	$T_{resp,8}$	0.024	s
$V_{t1,4}$	0.895	p.u.	$T_{resp,9}$	0.016	s
$V_{t1,5}$	0.885	p.u.	$T_{resp,10}$	0.002	s
$V_{t1,6}$	0.882	p.u.	$k_{p,PLL,1}$	91.9	Hz
$V_{t1,7}$	0.895	p.u.	$k_{p,PLL,2}$	66.2	Hz
$V_{t1,8}$	0.893	p.u.	$k_{p,PLL,3}$	97.9	Hz
$V_{t1,9}$	0.895	p.u.	$k_{p,PLL,4}$	67.6	Hz
$V_{t1,10}$	0.892	p.u.	$k_{p,PLL,5}$	68.1	Hz
$V_{t2,1}$	1.122	p.u.	$k_{p,PLL,6}$	65.9	Hz
$V_{t2,2}$	1.114	p.u.	$k_{p,PLL,7}$	68.5	Hz
$V_{t2,3}$	1.173	p.u.	$k_{p,PLL,8}$	70.1	Hz
$V_{t2,4}$	1.157	p.u.	$k_{p,PLL,9}$	71.8	Hz
$V_{t2,5}$	1.193	p.u.	$k_{p,PLL,10}$	79.0	Hz
$V_{t2,6}$	1.164	p.u.	$k_{i,PLL,1}$	1193.8	Hz
$V_{t2,7}$	1.135	p.u.	$k_{i,PLL,2}$	702.3	Hz
$V_{t2,8}$	1.102	p.u.	$k_{i,PLL,3}$	754.7	Hz
$V_{t2,9}$	1.181	p.u.	$k_{i,PLL,4}$	838.1	Hz
$V_{t2,10}$	1.153	p.u.	$k_{i,PLL,5}$	644.4	Hz
Ddn_1	0.338	$\frac{1}{Hz}\cdot$ p.u. on mbase	$k_{i,PLL,6}$	1010.5	Hz
Ddn_2	0.490	$\frac{1}{Hz}\cdot$ p.u. on mbase	$k_{i,PLL,7}$	841.4	Hz
Ddn_3	0.627	$\frac{1}{Hz}\cdot$ p.u. on mbase	$k_{i,PLL,8}$	1189.7	Hz
Ddn_4	0.358	$\frac{1}{Hz}\cdot$ p.u. on mbase	$k_{i,PLL,9}$	841.3	Hz
Ddn_5	0.702	$\frac{1}{Hz}\cdot$ p.u. on mbase	$k_{i,PLL,10}$	972.4	Hz
Ddn_6	0.571	$\frac{1}{Hz}\cdot$ p.u. on mbase	w_{c1}	42.71	rad/s
Ddn_7	0.294	$\frac{1}{Hz}\cdot$ p.u. on mbase	w_{c2}	48.96	rad/s
Ddn_8	0.818	$\frac{1}{Hz}\cdot$ p.u. on mbase	w_{c3}	54.74	rad/s
Ddn_9	0.251	$\frac{1}{Hz}\cdot$ p.u. on mbase	w_{c4}	44.75	rad/s
Ddn_{10}	0.412	$\frac{1}{Hz}\cdot$ p.u. on mbase	w_{c5}	44.90	rad/s
$T_{resp,1}$	0.007	s	w_{c6}	35.34	rad/s
$T_{resp,2}$	0.056	s	w_{c7}	32.18	rad/s
$T_{resp,3}$	0.011	s	w_{c8}	40.53	rad/s
$T_{resp,4}$	0.016	s	w_{c9}	41.39	rad/s
$T_{resp,5}$	0.048	s	w_{c10}	51.95	rad/s

A.3 Complexity level 15

Table A.5: Generated detailed model parameters complexity level 15 part 1/3

Parameter	Value	Unit	Parameter	Value	Unit
$P_{Lo,1}$	50.76	kW	$P_{DG,1}$	14.26	kW
$P_{Lo,2}$	13.51	kW	$P_{DG,2}$	1.71	kW
$P_{Lo,3}$	28.49	kW	$P_{DG,3}$	13.83	kW
$P_{Lo,4}$	21.84	kW	$P_{DG,4}$	10.99	kW
$P_{Lo,5}$	47.50	kW	$P_{DG,5}$	14.82	kW
$P_{Lo,6}$	29.99	kW	$P_{DG,6}$	9.33	kW
$P_{Lo,7}$	52.76	kW	$P_{DG,7}$	13.06	kW
$P_{Lo,8}$	18.14	kW	$P_{DG,8}$	8.78	kW
$P_{Lo,9}$	22.03	kW	$P_{DG,9}$	5.74	kW
$P_{Lo,10}$	16.41	kW	$P_{DG,10}$	2.50	kW
$P_{Lo,11}$	15.96	kW	$P_{DG,11}$	6.93	kW
$P_{Lo,12}$	50.79	kW	$P_{DG,12}$	13.68	kW.
$P_{Lo,13}$	37.04	kW	$P_{DG,13}$	7.67	kW
$P_{Lo,14}$	35.62	kW	$P_{DG,14}$	9.81	kW
$P_{Lo,15}$	16.39	kW	$P_{DG,15}$	2.39	kW
$Q_{Lo,1}$	16.69	kVar	$F_{t1,1}$	46.67	Hz
$Q_{Lo,2}$	4.44	kVar	$F_{t1,2}$	46.95	Hz
$Q_{Lo,3}$	9.36	kVar	$F_{t1,3}$	46.69	Hz
$Q_{Lo,4}$	7.18	kVar	$F_{t1,4}$	47.13	Hz
$Q_{Lo,5}$	15.61	kVar	$F_{t1,5}$	47.28	Hz
$Q_{Lo,6}$	9.86	kVar	$F_{t1,6}$	46.81	Hz
$Q_{Lo,7}$	17.34	kVar	$F_{t1,7}$	47.29	Hz
$Q_{Lo,8}$	5.96	kVar	$F_{t1,8}$	47.03	Hz
$Q_{Lo,9}$	7.24	kVar	$F_{t1,9}$	47.05	Hz
$Q_{Lo,10}$	5.39	kVar	$F_{t1,10}$	46.80	Hz
$Q_{Lo,11}$	5.25	kVar	$F_{t1,11}$	46.69	Hz
$Q_{Lo,12}$	16.69	kVar	$F_{t1,12}$	46.94	Hz
$Q_{Lo,13}$	12.17	kVar	$F_{t1,13}$	46.68	Hz
$Q_{Lo,14}$	11.71	kVar	$F_{t1,14}$	46.61	Hz
$Q_{Lo,15}$	5.39	kVar	$F_{t1,15}$	46.76	Hz

Table A.6: Generated detailed model parameters complexity level 15 part 2/3

Parameter	Value	Unit	Parameter	Value	Unit
$F_{t2,1}$	52.15	Hz	Ddn_1	0.846	$\frac{1}{Hz}\cdot$ p.u. on mbase
$F_{t2,2}$	52.05	Hz	Ddn_2	0.922	$\frac{1}{Hz}\cdot$ p.u. on mbase
$F_{t2,3}$	52.19	Hz	Ddn_3	0.273	$\frac{1}{Hz}\cdot$ p.u. on mbase
$F_{t2,4}$	52.28	Hz	Ddn_4	0.928	$\frac{1}{Hz}\cdot$ p.u. on mbase
$F_{t2,5}$	51.99	Hz	Ddn_5	0.694	$\frac{1}{Hz}\cdot$ p.u. on mbase
$F_{t2,6}$	52.00	Hz	Ddn_6	0.248	$\frac{1}{Hz}\cdot$ p.u. on mbase
$F_{t2,7}$	52.14	Hz	Ddn_7	0.399	$\frac{1}{Hz}\cdot$ p.u. on mbase
$F_{t2,8}$	51.85	Hz	Ddn_8	0.623	$\frac{1}{Hz}\cdot$ p.u. on mbase
$F_{t2,9}$	52.12	Hz	Ddn_9	0.965	$\frac{1}{Hz}\cdot$ p.u. on mbase
$F_{t2,10}$	51.97	Hz	Ddn_{10}	0.971	$\frac{1}{Hz}\cdot$ p.u. on mbase
$F_{t2,11}$	51.73	Hz	Ddn_{11}	0.298	$\frac{1}{Hz}\cdot$ p.u. on mbase
$F_{t2,12}$	51.81	Hz	Ddn_{12}	0.976	$\frac{1}{Hz}\cdot$ p.u. on mbase
$F_{t2,13}$	52.40	Hz	Ddn_{13}	0.964	$\frac{1}{Hz}\cdot$ p.u. on mbase
$F_{t2,14}$	51.76	Hz	Ddn_{14}	0.571	$\frac{1}{Hz}\cdot$ p.u. on mbase
$F_{t2,15}$	52.10	Hz	Ddn_{15}	0.834	$\frac{1}{Hz}\cdot$ p.u. on mbase
$V_{t1,1}$	0.895	p.u.	$T_{resp,1}$	0.046	s
$V_{t1,2}$	0.886	p.u.	$T_{resp,2}$	0.045	s
$V_{t1,3}$	0.884	p.u.	$T_{resp,3}$	0.024	s
$V_{t1,4}$	0.882	p.u.	$T_{resp,4}$	0.039	s
$V_{t1,5}$	0.889	p.u.	$\mathrm{T}_{resp,5}$	0.010	s
$V_{t1,6}$	0.890	p.u.	$T_{resp,6}$	0.042	s
$V_{t1,7}$	0.888	p.u.	$T_{resp,7}$	0.002	s
$V_{t1,8}$	0.899	p.u.	$T_{resp,8}$	0.017	s
$V_{t1,9}$	0.892	p.u.	$T_{resp,9}$	0.003	s
$V_{t1,10}$	0.885	p.u.	$T_{resp,10}$	0.006	s
$V_{t1,11}$	0.883	p.u.	$T_{resp,11}$	0.049	s
$V_{t1,12}$	0.899	p.u.	$\mathrm{T}_{resp,12}$	0.042	s
$V_{t1,13}$	0.900	p.u.	$T_{resp,13}$	0.019	s
$V_{t1,14}$	0.888	p.u.	$T_{resp,14}$	0.057	s
$V_{t1,15}$	0.894	p.u.	$T_{resp,15}$	0.002	s
$V_{t2,1}$	1.165	p.u.	$k_{p,PLL,1}$	76.6	Hz
$V_{t2,2}$	1.175	p.u.	$k_{p,PLL,2}$	100.8	Hz
$V_{t2,3}$	1.137	p.u.	$k_{p,PLL,3}$	99.3	Hz
$V_{t2,4}$	1.193	p.u.	$k_{p,PLL,4}$	69.8	Hz
$V_{t2,5}$	1.145	p.u.	$k_{p,PLL,5}$	67.1	Hz
$V_{t2,6}$	1.181	p.u.	$k_{p,PLL,6}$	89.9	Hz
$V_{t2,7}$	1.181	p.u.	$k_{p,PLL,7}$	117.6	Hz
$V_{t2,8}$	1.188	p.u.	$k_{p,PLL,8}$	80.4	Hz
$V_{t2,9}$	1.123	p.u.	$k_{p,PLL,9}$	95.1	Hz
$V_{t2,10}$	1.184	p.u.	$k_{p,PLL,10}$	73.4	Hz
$V_{t2,11}$	1.123	p.u.	$k_{p,PLL,11}$	105.1	Hz
$V_{t2,12}$	1.143	p.u.	$k_{p,PLL,12}$	75.3	Hz
$V_{t2,13}$	1.144	p.u.	$k_{p,PLL,13}$	90.4	Hz
$V_{t2,14}$	1.160	p.u.	$k_{p,PLL,14}$	101.9	Hz
$V_{t2,15}$	1.122	p.u.	$k_{p,PLL,15}$	113.5	Hz

Table A.7: Generated detailed model parameters complexity level 15 part 3/3

Parameter	Value	Unit	Parameter	Value	Unit
$k_{i,PLL,1}$	810.0	Hz	w_{c1}	31.51	rad/s
$k_{i,PLL,2}$	718.0	Hz	w_{c2}	56.37	rad/s
$k_{i,PLL,3}$	750.7	Hz	w_{c3}	41.19	rad/s
$k_{i,PLL,4}$	969.6	Hz	w_{c4}	48.02	rad/s
$k_{i,PLL,5}$	884.0	Hz	w_{c5}	36.62	rad/s
$k_{i,PLL,6}$	811.0	Hz	w_{c6}	50.33	rad/s
$k_{i,PLL,7}$	1098.5	Hz	w_{c7}	39.68	rad/s
$k_{i,PLL,8}$	951.2	Hz	w_{c8}	51.96	rad/s
$k_{i,PLL,9}$	929.8	Hz	w_{c9}	53.07	rad/s
$k_{i,PLL,10}$	1150.3	Hz	w_{c10}	54.92	rad/s
$k_{i,PLL,11}$	771.5	Hz	w_{c11}	45.57	rad/s
$k_{i,PLL,12}$	1054.3	Hz	w_{c12}	34.05	rad/s
$k_{i,PLL,13}$	1052.2	Hz	w_{c13}	38.61	rad/s
$k_{i,PLL,14}$	828.3	Hz	w_{c14}	60.11	rad/s
$k_{i,PLL,15}$	940.7	Hz	w_{c15}	36.20	rad/s

Appendix B

Identified equivalent model parameters

B.1 Training for a frequency deviation of -3Hz

Table B.1: Identified parameters for training for a frequency deviation of -3Hz

Parameter	Value	Unit
F_{pt0}	46.50	Hz
F_{pt1}	47.38	Hz
F_{pt2}	51.79	Hz
F_{pt3}	52.29	Hz
V_{pt0}	0.880	p.u.
V_{pt1}	0.897	p.u.
V_{pt2}	1.133	p.u.
V_{pt3}	1.156	p.u.
Ddn	0.638	$\frac{1}{Hz}\cdot$ p.u. on mbase
T_{resp}	0.0092	s
$k_{p,PLL}$	1932	Hz
$k_{i,PLL}$	64.79	Hz
w_c	60.47	rad/s

B.2 Training for a voltage deviation of 0.23p.u.

Table B.2: Identified parameters for training for a voltage deviation of 0.23p.u.

Parameter	Value	Unit
F_{pt0}	46.58	Hz
F_{pt1}	47.04	Hz
F_{pt2}	51.59	Hz
F_{pt3}	52.09	Hz
V_{pt0}	0.881	p.u.
V_{pt1}	0.898	p.u.
V_{pt2}	1.129	p.u.
V_{pt3}	1.182	p.u.
Ddn	0.496	$\frac{1}{Hz}\cdot$ p.u. on mbase
T_{resp}	0.0328	s
$k_{p,PLL}$	876.3	Hz
$k_{i,PLL}$	98.7	Hz
w_c	38.56	rad/s

B.3 Training for several faults

B.3.1 Complexity level 5

Table B.3: Identified parameters for training for several faults for the complexity level 5 case

Parameter	Value	Unit
F_{pt0}	46.50	Hz
F_{pt1}	47.50	Hz
F_{pt2}	51.61	Hz
F_{pt3}	51.71	Hz
V_{pt0}	0.871	p.u.
V_{pt1}	0.918	p.u.
V_{pt2}	1.159	p.u.
V_{pt3}	1.191	p.u.
Ddn	0.575	$\frac{1}{Hz}\cdot$ p.u. on mbase
T_{resp}	0.0071	s
$k_{p,PLL}$	113.3	Hz
$k_{i,PLL}$	1199	Hz
w_c	42.13	rad/s

B.3.2 Complexity level 10

Table B.4: Identified parameters for training for several faults for the complexity level 10 case

Parameter	Value	Unit
F_{pt0}	46.53	Hz
F_{pt1}	47.40	Hz
F_{pt2}	52.02	Hz
F_{pt3}	52.22	Hz
V_{pt0}	0.896	p.u.
V_{pt1}	0.897	p.u.
V_{pt2}	1.103	p.u.
V_{pt3}	1.191	p.u.
Ddn	0.474	$\frac{1}{Hz}\cdot$ p.u. on mbase
T_{resp}	0.0380	s
$k_{p,PLL}$	100.1	Hz
$k_{i,PLL}$	1135	Hz
w_c	45.37	rad/s

B.3.3 Complexity level 15

Table B.5: Identified parameters for training for several faults for the complexity level 15 case

Parameter	Value	Unit
F_{pt0}	46.51	Hz
F_{pt1}	47.33	Hz
F_{pt2}	52.24	Hz
F_{pt3}	52.33	Hz
V_{pt0}	0.884	p.u.
V_{pt1}	0.898	p.u.
V_{pt2}	1.109	p.u.
V_{pt3}	1.139	p.u.
Ddn	0.575	$\frac{1}{Hz}\cdot$ p.u. on mbase
T_{resp}	0.0318	s
$k_{p,PLL}$	75.3	Hz
$k_{i,PLL}$	1052	Hz
w_c	48.56	rad/s

Appendix C

Simulation time measurements

C.1 Complexity level 5

	Simulation time (s)		Comparison	
Fault	Detailed model	Reduced-order model	Difference (s)	Reduction (%)
−4.0 Hz	27.24	4.72	22.53	82.7
−2.5 Hz	21.22	5.29	15.93	75.1
+0.2 Hz	21.55	4.28	17.27	80.1
+1.6 Hz	21.11	4.19	16.92	80.2
+3.0 Hz	20.51	4.37	16.14	78.7
−0.19 p.u.	18.29	4.28	14.01	76.6
−0.07 p.u.	19.15	4.69	14.46	75.5
+0.06 p.u.	23.05	4.59	18.46	80.1
+0.14 p.u.	22.57	4.87	17.70	78.4
+0.37 p.u.	18.75	4.78	13.97	74.5
Mean	21.34	4.61	16.74	**78.4**

Table C.1: Simulation time comparison for the complexity level 5

C.2 Complexity level 10

	Simulation time (s)		Comparison	
Fault	Detailed model	Reduced-order model	Difference (s)	Reduction (%)
−4.0 Hz	34.30	3.22	31.08	90.6
−2.5 Hz	48.22	4.32	43.90	91.4
+0.2 Hz	47.51	4.32	43.19	90.9
+1.6 Hz	46.73	4.03	42.70	91.4
+3.0 Hz	46.66	4.20	42.46	91.0
−0.19 p.u.	41.56	4.21	37.35	89.9
−0.07 p.u.	40.14	4.19	35.95	89.6
+0.06 p.u.	45.05	4.71	40.34	89.5
+0.14 p.u.	55.61	4.32	51.29	92.2
+0.37 p.u.	49.69	4.39	45.30	91.2
Mean	45.55	4.19	41.36	**90.8**

Table C.2: Simulation time comparison for the complexity level 10

C.3 Complexity level 15

	Simulation time (s)		Comparison	
Fault	Detailed model	Reduced-order model	Difference (s)	Reduction (%)
−4.0 Hz	60.29	4.30	55.99	92.9
−2.5 Hz	70.97	4.50	66.47	93.7
+0.2 Hz	69.03	4.32	64.71	93.7
+1.6 Hz	70.05	4.29	65.76	93.9
+3.0 Hz	71.10	4.42	66.68	93.8
−0.19 p.u.	69.29	4.34	64.95	93.7
−0.07 p.u.	65.04	4.42	60.62	93.2
+0.06 p.u.	67.34	4.39	62.95	93.5
+0.14 p.u.	71.57	4.35	67.22	93.9
+0.37 p.u.	71.62	4.43	67.19	93.8
Mean	68.63	4.38	64.25	**93.6**

Table C.3: Simulation time comparison for the complexity level 15

UNIVERSITÉ CATHOLIQUE DE LOUVAIN
École polytechnique de Louvain
Rue Archimède, 1 bte L6.11.01, 1348 Louvain-la-Neuve, Belgique | **www.uclouvain.be/epl**